Widespread transneuronal propagation of α-synucleinopathy triggered in olfactory bulb mimics prodromal Parkinson's disease

Nolwen L. Rey,[1] Jennifer A. Steiner,[1] Nazia Maroof,[1,3] Kelvin C. Luk,[4] Zachary Madaj,[2] John Q. Trojanowski,[4] Virginia M.-Y. Lee,[4] and Patrik Brundin[1]

[1]Center for Neurodegenerative Science and [2]Bioinformatics and Biostatistics Core, Van Andel Research Institute, Grand Rapids, MI 49503
[3]Roche Pharma Research & Early Development, Neuroscience Discovery, Roche Innovation Center, 4070 Basel, Switzerland
[4]Department of Pathology and Laboratory Medicine, Institute on Aging and Center for Neurodegenerative Disease Research, University of Pennsylvania, Philadelphia, PA 19104

Parkinson's disease (PD) is characterized by the progressive appearance of intraneuronal Lewy aggregates, which are primarily composed of misfolded α-synuclein (α-syn). The aggregates are believed to propagate via neural pathways following a stereotypical pattern, starting in the olfactory bulb (OB) and gut. We hypothesized that injection of fibrillar α-syn into the OB of wild-type mice would recreate the sequential progression of Lewy-like pathology, while triggering olfactory deficits. We demonstrate that injected α-syn fibrils recruit endogenous α-syn into pathological aggregates that spread transneuronally over several months, initially in the olfactory network and later in distant brain regions. The seeded inclusions contain post-translationally modified α-syn that is Thioflavin S positive, indicative of amyloid fibrils. The spreading α-syn pathology induces progressive and specific olfactory deficits. Thus, we demonstrate that propagating α-syn pathology triggered in the OB is functionally detrimental. Collectively, we have created a mouse model of prodromal PD.

INTRODUCTION

Misfolded α-synuclein (α-syn) accumulates in Lewy bodies (in somata) and Lewy neurites, which are intraneuronal inclusions found in Parkinson's disease (PD; Goedert, 2001). In both PD (Goedert, 2001; Braak et al., 2003b) and other Lewy body disorders (Beach et al., 2009), pathological α-syn inclusions progressively develop in a spatially stereotypic pattern in the brain that appears to follow neuronal connections. Braak et al. (2003b) suggested that PD pathology initially develops in anterior olfactory regions, the enteric nervous system and the dorsal motor nucleus of the vagus nerve (DMX), before spreading to different brain regions via axonal projections.

Significant nervous system pathology is suggested to be present several years before PD diagnosis and onset of the classical motor syndrome (i.e., tremor, rigidity, and bradykinesia; Mahlknecht et al., 2015). During this phase, termed prodromal PD, certain nonmotor signs are evident, e.g., olfactory dysfunction, rapid eye movement sleep behavior disorder, constipation, and other autonomic disturbances (Postuma et al., 2012; Mahlknecht et al., 2015). Prodromal PD is viewed as the ideal stage at which to apply neuroprotective and disease-modifying strategies. To facilitate development of such therapies, improved understanding of PD etiology and the route of pathology spread between different parts of the nervous system is necessary. The prion-like propagation theory for PD suggests that misfolded α-syn seeds aggregation of natively unfolded α-syn (Olanow and Prusiner, 2009; George et al., 2013; Guo and Lee, 2014). Such misfolded α-syn is then potentially transported over long distances in axons, released into the extracellular space and taken up by neighboring cells (Dunning et al., 2012; Lamberts et al., 2014). This process is proposed to contribute to the spatial progression of PD pathology. α-Syn pathology can be triggered in experimental animals after intracerebral, intramuscular, or intravenous inoculation of brain homogenates from affected mice and patients, or recombinant fibrillar α-syn (Luk et al., 2012a,b; Mougenot et al., 2012; Masuda-Suzukake et al., 2013; Recasens et al., 2014; Sacino et al., 2014; Paumier et al., 2015; Peelaerts et al., 2015; Dehay et al., 2016). The pathology appears in brain regions anatomically connected to the injection site, but observations of pathology that progressively involves synaptically connected neurons in different brain regions are lacking (Rey

Correspondence to Nolwen L. Rey: Nolwen.Rey@vai.org

Abbreviations used: α-syn, α-synuclein; ACC, anterior cingulate area; Am B, basal amygdaloid nuclei; Am Co, cortical amygdaloid nuclei and areas; AON, anterior olfactory nucleus; AP, propionic acid; Contra, contralateral; DMX, dorsal motor nucleus of the vagus nerve; Ect, Ectorhinal cortex; Ent, entorhinal cortex; FC, frontal and orbital cortex; Hipp, hippocampus; HuPFFs, human PFF; LC, locus coeruleus; LMMs, linear mixed-effects model; mMs, mouse monomeric α-syn; MO, mineral oil; Mol, molecular layer of the hippocampus; mPFFs, preformed fibrils of recombinant mouse α-syn; nLOT, nucleus of the lateral olfactory tract; OB, olfactory bulb; OT, olfactory tubercle; PC, piriform cortex; PD, Parkinson's disease; PFFs, pre-formed fibrillar assemblies of recombinant α-synuclein; PRh, perirhinal cortex; Pser129, α-syn phosphorylated on serine 129; RN, raphe nucleus; SN, substantia nigra; ThS, Thioflavin S.

The Rockefeller University Press $30.00
J. Exp. Med. 2016 Vol. 213 No. 9 1759–1778
www.jem.org/cgi/doi/10.1084/jem.20160368

et al., 2016). Most prior studies are on misfolded α-syn injected in transgenic mice overexpressing α-syn, and few have used WT mice (Dehay et al., 2016). Importantly, no prior study has focused on the olfactory system, which is highly relevant to prodromal PD and might represent a trigger site for α-syn pathology (Braak et al., 2003b; Beach et al., 2009).

We now demonstrate that α-syn pathology, resembling human disease, propagates sequentially between synaptically connected brain regions 1–12 mo after α-syn fibril injection into the olfactory bulb (OB), and eventually reaches multiple structures that display Lewy pathology in PD. We also reveal progressive olfactory deficits in the mice inoculated with α-syn fibrils. We suggest that injections of α-syn fibrils into mouse OB result in a novel model of prodromal PD that can be used to test therapeutics aimed at preventing or slowing PD development.

RESULTS

We hypothesized that injection of fibrillar α-syn into the OB of WT mice would trigger stereotypic progression of induced α-syn–positive pathology and replicate features of the neuropathology that has been associated with prodromal PD. We tested this hypothesis by stereotactically injecting preformed fibrillar assemblies of recombinant α-syn (PFFs; Luk et al., 2012a; Volpicelli-Daley et al., 2014). We used fibrils of either human (HuPFFs) or mouse (mPFFs) α-syn, and injected WT mice unilaterally into the OB following a previously published surgical protocol (Rey et al., 2013). Importantly, this volume of injectate does not lead to diffusion into cerebrospinal fluid or brain parenchyma adjacent to the OB (Rey et al., 2013).

Uptake of PFFs and induction of α-synucleinopathy in the OB

As we had predicted, 90 min after injection of HuPFFs, mitral cells, i.e., the relay cells of the OB (βIII-tubulin-positive [Tuj1] in confocal images), contain HuPFFs (human α-syn immunoreactivity; Fig. 1, A–C), indicating immediate uptake of PFFs by mitral cells of the OB. 1 mo after injection, we detected α-syn–immunoreactive pathology using an antibody directed against α-syn phosphorylated on serine 129 (Pser129), the predominant posttranslational modification of α-syn occurring in synucleinopathies (Fujiwara et al., 2002; Oueslati, 2016). Antiserum directed against Pser129 labels abnormal α-syn inclusions and is a reliable marker for α-syn pathology (Beach et al., 2009; Rey et al., 2016). We detected Pser129-immunoreactive material both in mitral cell bodies and in neurites in the OB of mice injected with HuPFFs or mPFFs (Fig. 1, D and E). Control injections (PBS) or mouse monomeric α-syn (mMs) did not induce Pser129 pathology in the OB (Fig. 1, F and G). To define the consequences of injections of PFFs, we quantified mitral cells at the injection site 6 mo after injection. Measurements of mitral cell density in the OB reveal no neuronal loss (Fig. 1, H and I).

Widespread progressive propagation of mPFFs α-synucleinopathy along anatomical pathways

To assess the propagation of pathology in mouse brain, we analyzed Pser129-immunostained sections and examined the entire brain 1–12 mo after injection in noninjected, PBS-, mMs-, HuPFFs-, and mPFFs-injected mice. Presence of a single Pser129-positive cell or neurite was considered pathological, akin to how, Lewy pathology distribution is staged in human brain (Braak et al., 2003a,b; Beach et al., 2009). 1 mo after unilateral injection of mPFFs in the OB, we found Pser129 α-syn in widespread areas anatomically connected to the OB (Figs. 2 A and 3). They included ipsilateral piriform cortex (PC), entorhinal cortex (Ent), cortical amygdaloid nuclei and areas (Am Co), and ipsilateral and contralateral anterior olfactory nucleus (AON), which are all part of the olfactory system, and either receive direct axonal projections from the mitral cells and/or send direct efferents to the OB (Doty, 2003), as well as in the basolateral amygdala, which sends inputs to the Ent (Fig. 2 A). Importantly, we did not observe pathology in the control mice (uninjected or injected with mMs) at any time point up to 12 mo after injection (Fig. 3).

At 3 mo, the Pser129 pathology progressed to additional areas located 1 synapse away from those directly connected with the injected OB. Those structures included the molecular layer of hippocampus (Mol(Hipp)), which receives afferent projections from Ent (De La Rosa-Prieto et al., 2015); the insulate cortex, which receives inputs from the amygdala (Shi and Cassell, 1998); Ect, which receives projections from Ent (Burwell et al., 1995); other basal amygdaloid nuclei (Am B; Sah et al., 2003); and frontal and orbital cortex (FC; Cinelli et al., 1987; Figs. 2 B and 3). In short, in the ipsilateral hemisphere at 3 mo, pathology was only present in structures that send or receive direct projections from olfactory regions. At this time, α-syn pathology was also present in contralateral olfactory structures connected to the contralateral AON, which already exhibited α-syn aggregates 1 mo after injection.

At 6 mo, we observed Pser129 pathology in additional brain areas that are directly connected to the OB, including nucleus of the lateral olfactory tract (nLOT) and the olfactory tubercle (OT). We also detected pathology outside the olfactory system, two synapses away from the OB, in, e.g., the central amygdala and the dentate gyrus, and cornu ammonis of the Hipp (Figs. 2 C and 3). We also observed α-syn pathology in other central brain regions, e.g., the thalamus and hypothalamus.

Finally, at the 12-mo time point, mPFFs-induced Pser129 pathology was even more widespread. Cortical associative and secondary cortical brain regions (secondary visual [V2] and somatosensory [S2] cortices and the anterior cingulate area [ACC]) exhibited pathology (Figs. 2 D and 3). Occasionally, we found Pser129 immunoreactivity in the locus coeruleus (LC), the substantia nigra (SN), and the medial and dorsal raphe nuclei (RN).

In total, we detected α-syn pathology in >40 brain regions or subregions at 12 mo after injection. Additional micrographs

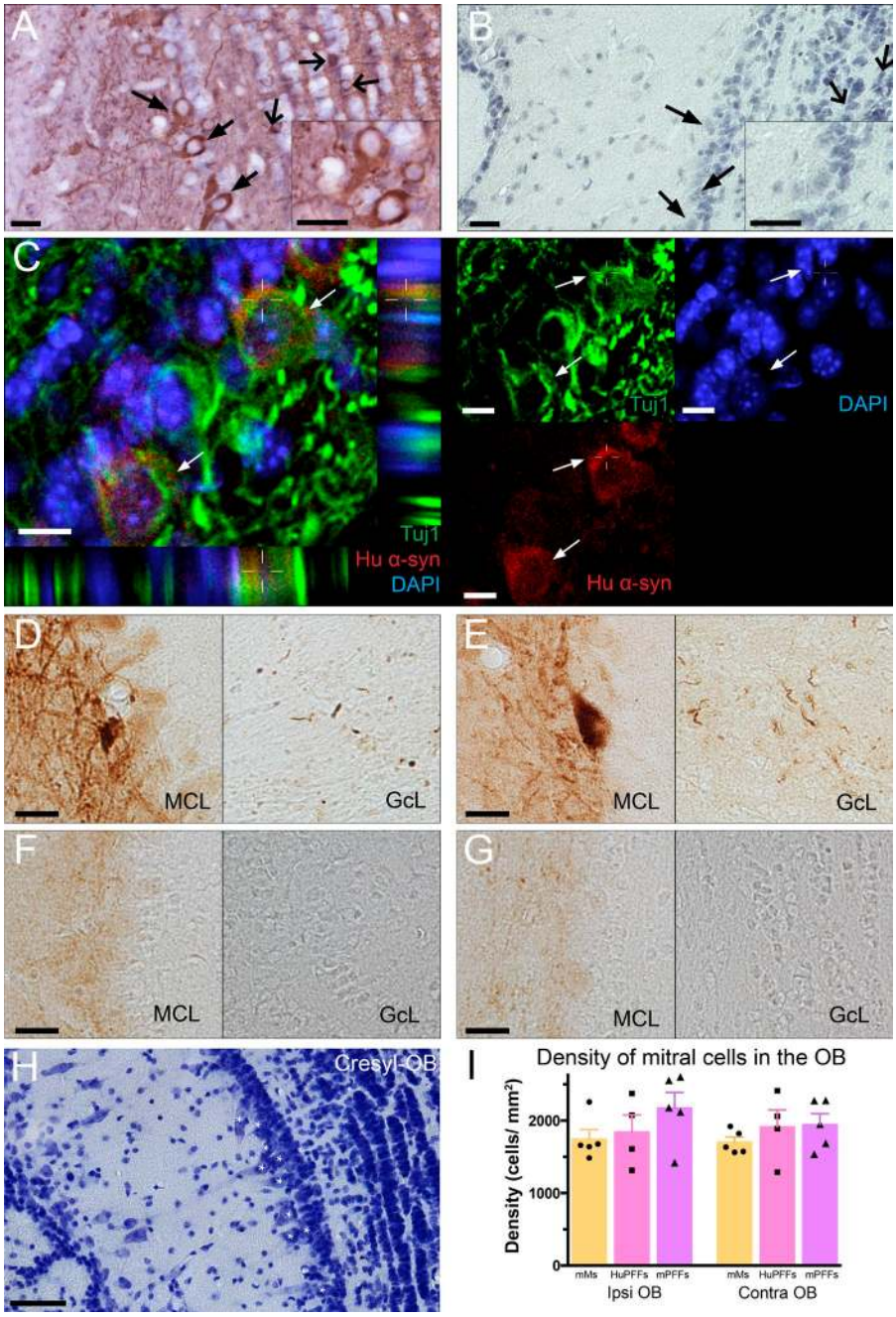

Figure 1. **PFFs injected in the OB of WT mice were rapidly taken up by mitral cells and induced α-syn pathology after 1 mo.** (A and B) Mitral cells (plain black arrows; cells delineated in B) and granule cells (simple wide black arrows) were positive for human α-syn 1.5 h after injection of HuPFFs in the OB (A), but not in noninjected animals (B). (C) 1.5 h after injection, human α-syn (red) was detected within mitral cells (Tuj1-positive, green DAPI, blue; white arrows). (D–G) α-Syn pathology detected by an antibody directed against α-syn phosphorylated on serine 129 (Pser129) can be observed in mitral cells in the mitral cell layer (MCL) and the granule cell layer (GcL) of OB 1 mo after injection of HuPFFs (D) or mouse PFFs (mPFFs; E), but not after injection of mouse monomers (mMs; F) or PBS (G). (A–G) Histochemical analysis was performed on all animals euthanized 1.5 h after HuPFFs injection in one histochemical experiment (A–C; $n = 4$ per group), and in six independent histochemical experiments on all animals euthanized 1, 3, 6, and 12 mo after injection of PBS, mMs, HuPFFs, and mPFFs (D–G; $n = 4$–5 per group). The data shown are from one representative animal. (H) Cresyl staining in the OB from one representative animal. White stars mark mitral cells. (I) Density of mitral cells in the mitral cell layer of the OB ($n = 4$–5 animals per group, performed on all animals from the 1-, 3-, and 6-mo survival time points; Ipsi, ipsilateral; Contra, contralateral). Data were analyzed by Kruskal–Wallis testing. No significant differences were observed ($P = 0.41$). Bars: (A and B) 20 µm; (C) 10 µm; (D–G) 20 µm; (H) 50 µm.

and a table listing brain regions with pathology are presented in Fig. 3 and Table S1 (abbreviations listed in Table S3).

Differential effect of mPFFs versus huPFFs injection on the extent of pathology

Next, we compared the spread of HuPFFs-induced pathology to that of the mPFFs. 1 mo after injection of HuPFFs, we found a similar pattern of Pser129 pathology in olfactory structures to that observed with mPFFs injections (Fig. 4 A). At 3 mo, the induced pathology spread into a limited number of areas located 1 synapse away from the olfactory system, including ipsilateral Hipp, basal amygdala (Am B), and to the contralateral PC (Fig. 4 B). At 6 mo, we observed Pser129 pathology in areas located two synapses away from the OB, but for HuPFFs-injected mice it was restricted to ipsilateral ectorhinal cortex (Ect) and contralateral Ent (Fig. 4 C). Finally, at the 12-mo time point, HuPFFs-induced Pser129 pathology spread to additional brain regions, some located two synapses away from the OB, but the pathology was less pronounced (Fig. 4 D) compared with mPFFs-injected mice (Fig. 2 D). The limited amount and spread of pathology in the HuPFFs mice can be appreciated in diagrams (Fig. 4, E–H), when com-

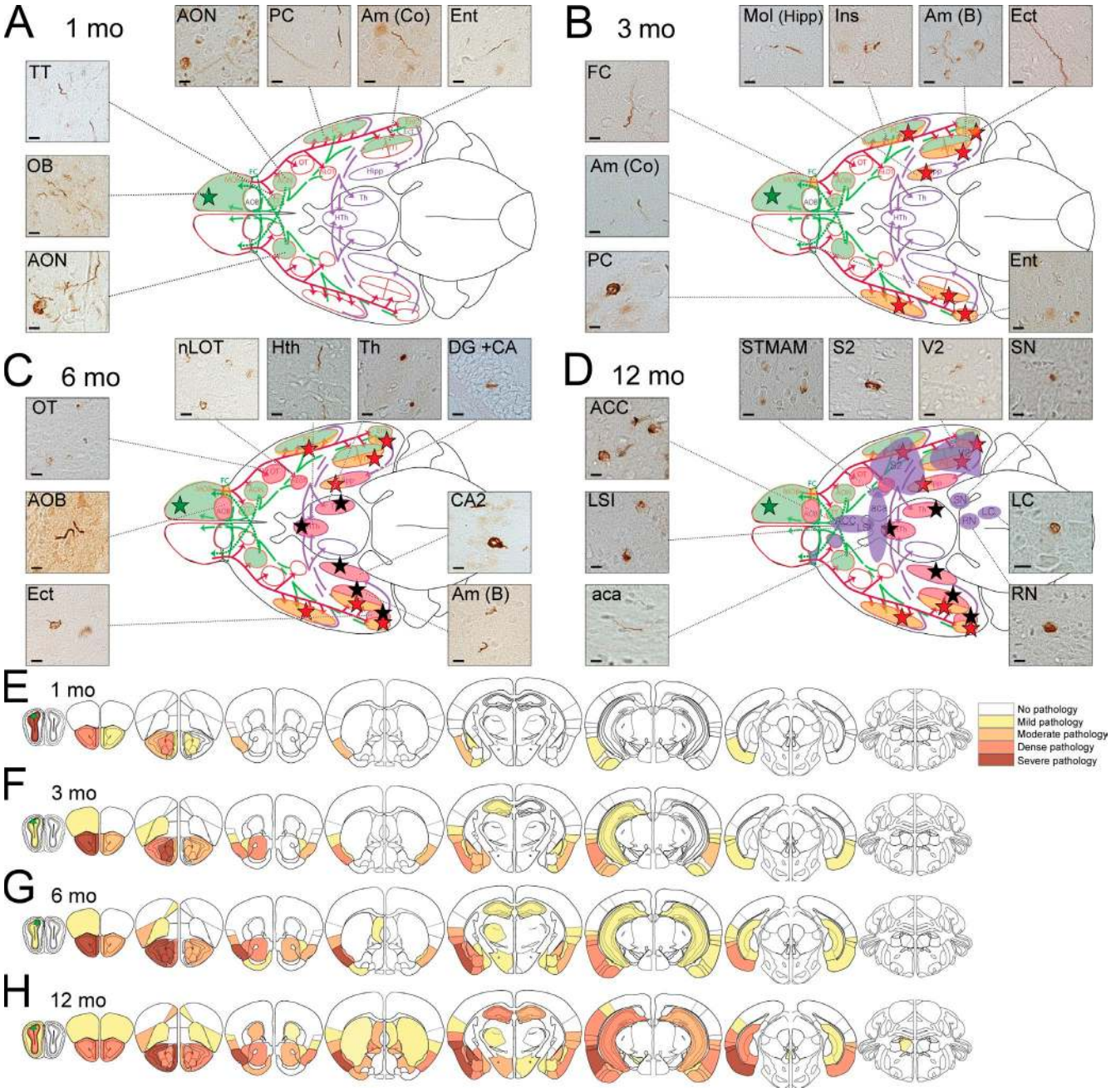

Figure 2. **mPFFs injected in OB caused progressive spreading of α-syn pathology first to olfactory structures, then to connected brain regions.** (A–D) Schematic of a ventral brain view. First and second order projections from and to the OB are depicted, respectively, in a red solid line, purple-dashed line, and green-dashed line. Colored regions represent brain structures where mPFFs-induced pathology appears (Pser129) at 1 mo (A, green regions), 3 mo (B, orange regions), 6 mo (C, pink regions), and 12 mo (D, purple regions) after injection. Micrographs show pathology (Pser129) in related brain regions. Location of injection is indicated with a green star. A list of the abbreviations is available as Table S3. The sections were immunostained in eight independent histochemical experiments. Histochemical analysis was performed on all animals from the 1-, 3-, 6-, and 12-mo survival time points; 1 and 3 mo delay, $n = 4$ mice per group; 6 and 12 mo delay, $n = 5$ mice per group. (A) At 1 mo delay, pathology was observed in olfactory regions (ipsi AON, PC, Am Co, Ent, TT, OB, and contra AON; Table S3). (B) Pathology was detected in additional brain regions after 3 mo (including ipsi FC, Mol, Am B, Ect, and contra Am Co, PC, and Ent). Regions located one synapse away from the olfactory system are identified with a red star. (C) Pathology was detected in additional brain regions after 6 mo (including ipsi nLOT, hypothalamus, thalamus, Hipp, OT, AOB, and contra CA2, AmB, and Ect). Brain regions located two synapses away from the olfactory system are labeled by a black star. (D) 12 mo after injection, additional brain regions displayed pathology. (E–H) Diagram illustrating the anatomical pattern of α-syn pathology in the brain on coronal sections 1 (E), 3 (F), 6 (G), and 12 mo (H) after injection. Bars: (A–D) 10 µm.

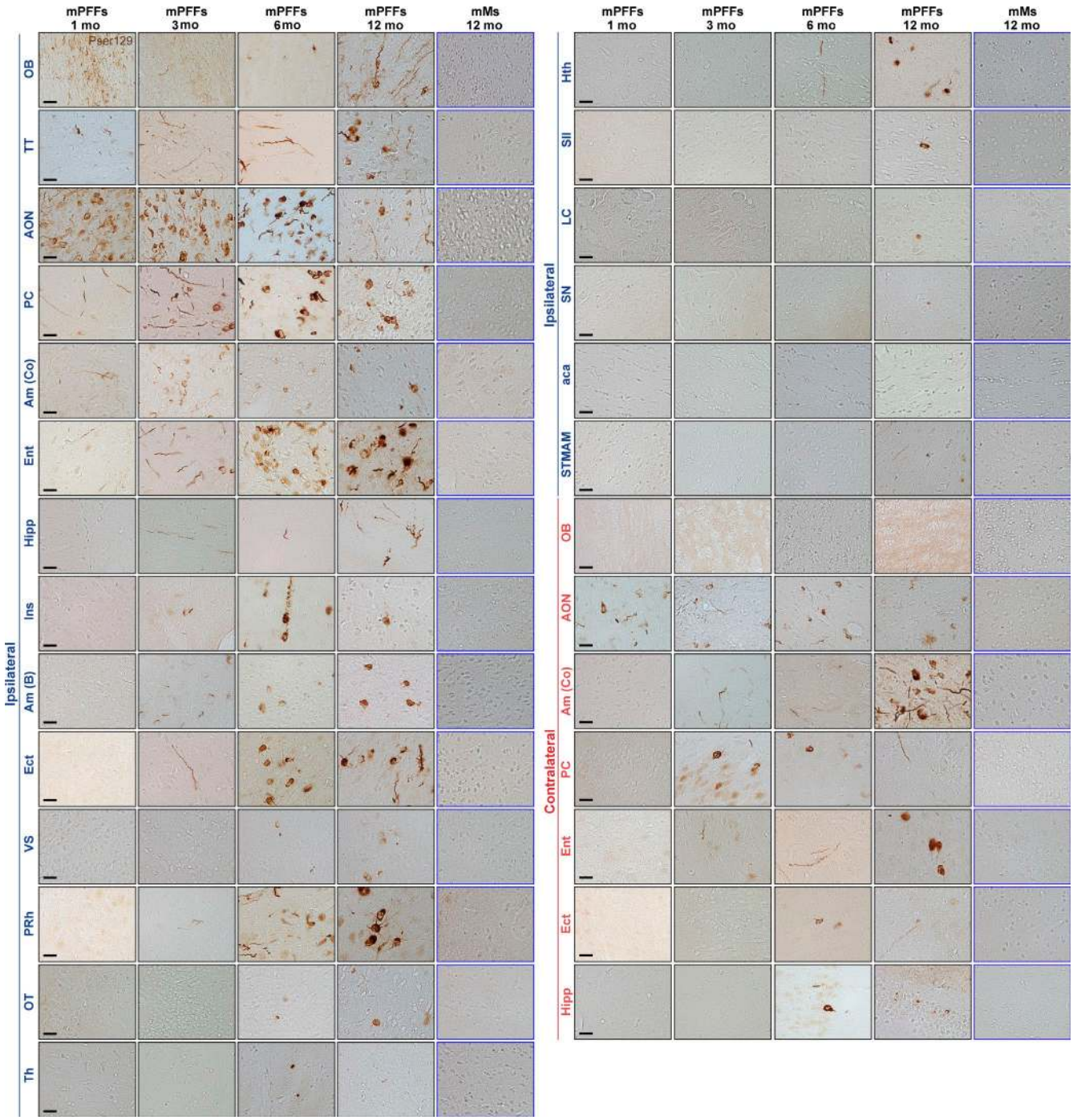

Figure 3. **Injection of mPFFs in the OB induced widespread α-syn pathology (Pser129) in the brain.** Pathology (Pser129) detected in numerous brain regions from 1 to 12 mo after injection of mPFFs in ipsilateral (Ipsi) and contralateral (Contra) structures. Histochemical analysis was performed on all animals from the 1-, 3-, 6-, 12-mo survival time points. The sections were immunostained in eight independent histochemical experiments. $n = 4–5$ animals per group. The data shown are from representative animals. List of abbreviations is available in Table S3. Bars: 20 µm.

pared with mPFFs (Fig. 2, E–H). The brain regions exhibiting pathology are listed in Tables S1 and S2. We then semi-quantitatively scored the pathology in mPFFs- and HuPFFs-injected mice in particular brain areas (AON, perirhinal cortex [PRh] and Ect) at 1, 3, and 6 mo. At all time points, there was no difference between mPFFs- and HuPFFs-injected mice in AON (Fig. 4, I–K). A trend toward more pathology in PRh was observed at 3 and 6 mo after injection, and significantly

more pathology was induced in Ect by mPFFs when compared with HuPFFs at 6 mo after injection. Collectively, in the long-term, the Pser129 pathology induced by injection of HuPFFs is not as extensive as that of mPFFs.

Characterization of the inclusions induced by PFFs injections

Next, we used confocal microscopy to characterize the inclusions induced by mPFFs with molecular markers typically used to evaluate Lewy pathology in human disease. 1 mo after injection, Pser129-positive inclusions in the AON co-localized with p62 (Fig. 5 A) and ubiquitin (Fig. 5 B), which are both characteristic of compact Lewy inclusions in PD (Kuusisto et al., 2003). The mPFFs-induced inclusions were also positive for Thioflavin S (ThS; Fig. 5, C–F), which binds to β-pleated sheets with cross β-secondary structure (Kelly, 1996), and detects proteins displaying an amyloid conformation (Li et al., 2010; Chu and Kordower, 2015). The ThS inclusions were resistant to proteinase K (Fig. 5, C–F, bottom). Thus, very mature α-syn amyloid inclusions were present at all time points from 1 to 12 mo after injection.

As it was previously suggested that misfolded α-syn can cross-seed with other amyloidogenic proteins (Giasson et al., 2003; Ishizawa et al., 2003; Guo et al., 2013; Moussaud et al., 2014), we used two antibodies detecting hyperphosphorylated tau, CP13 and PHF1 (Ishizawa et al., 2003) to determine whether mPFFs also induced tau pathology. We did not find any evidence of tau pathology in the AON or the PC 12 mo after injection (not depicted). We then characterized the cell types displaying Pser129-α-syn pathology 1 mo after injection of mPFFs. As expected, NeuN-positive cells (Fig. 5 G) contained Pser129 pathology. However, Iba-1–positive microglial cells (Fig. 5 H), GFAP-positive astrocytes (Fig. 5 I), and Olig-2/APC CC1-positive oligodendrocytes (Fig. 5 J) lacked Pser129 signal in the AON. We obtained similar results for HuPFFs-induced inclusions (Fig. 6).

To define the pathological consequences of injections of PFFs, we assessed neuroinflammation in the AON (Fig. 7 A). Qualitative analyses of the densities of Iba1-positive microglia revealed that there were no statistically significant differences between any of the groups (Fig. 7 B).

Specific and progressive olfactory deficits after PFFs injection

We also investigated extensively whether the pathology was associated with behavioral deficits. Open-field testing did not reveal gross motor or anxiety-related deficits (Fig. 8, A–F). Given the preponderance of pathology in the olfactory system, we conducted a battery of olfactory tests (odor detection, odor discrimination, and odor retention tests, adapted from previous studies; Mandairon et al., 2009; Rey et al., 2012a,b). No deficits were observed during the spontaneous odor discrimination test (Fig. 8 G). We also did not observe alteration of spontaneous habituation (first phase during the detection and discrimination tests; Figs. 8 G and 9). On the contrary, significant deficits were observed in other tests of olfactory function. In the odor detection test, the injection of mPFFs induced a lower odor detection threshold ($>10^{-2}$ dilution factor) already at 3 mo after injection, while injection of HuPFFs or mMs did not impact the odor detection threshold (Fig. 9 and Table S4). Odor retention time was significantly reduced (from 30 min in the control groups to 16 min in PFFs groups) 1 mo after injection of mPFFs or HuPFFs. The most severe deficits were induced by mPFFs that markedly reduced odor retention (<6 min) after 3 mo, whereas this level was achieved at 12 mo by HuPFFs (Fig. 10 and Table S4).

These data demonstrate that pathology induced by PFFs injection into OB leads to specific olfactory deficits that progressively increase, and which are more pronounced and rapidly developing in mPFFs-injected mice than in HuPFFs-injected mice.

DISCUSSION

We used carefully controlled local injections of fibrillar α-syn (Rey et al., 2013) to trigger α-synucleinopathy in the OB of WT mice. Over the 12 mo after injection, we found that the α-synucleinopathy gradually spread from the OB to multiple olfactory and nonolfactory brain regions that are also progressively affected in PD. At the longest follow-up period, we observed α-syn inclusions in neocortical brain regions, as well as occasionally in SN, RN, and LC neurons. This propagation is particularly striking considering that the injected mice do not overexpress α-syn and structures located several synapses away from the injection site are gradually affected. It also mimics the progression of α-syn pathology thought to occur in the olfactory system in prodromal PD. We also showed that the α-syn aggregates in affected neurons had several features—including immunoreactivity for ubiquitin, p62, and Pser129 α-syn, resistance to proteinase K, and ThS staining—that are characteristic of Lewy pathology seen in human disease.

Widespread progressive propagation of mPFFs α-synucleinopathy along anatomical pathways

The injection of PFFs in the OB triggered pathology first in ipsilateral olfactory regions connected to the site of injection, and spread to contralateral side, first in the contralateral AON. The contralateral AON is connected to both OBs (Brunjes and Illig, 2009; Illig and Eudy, 2009), therefore, the contralateral AON might play the role of a gateway through which misfolded α-syn can reach olfactory structures in the hemisphere contralateral to the injection. Later, pathology progressed to other ipsilateral and contralateral regions located one to two synapses away from the olfactory system. Interestingly, despite their spatial proximity and direct axonal connections to the OB, OT, and nLOT developed pathology later than other olfactory regions located at a similar distance from the injection site. These findings are consistent with observations of Lewy pathology in PD, where the OT and nLOT also develop pathology later than other olfactory structures (Del Tredici and Braak, 2000). This might indicate that those neurons are less prone to develop α-syn aggregates.

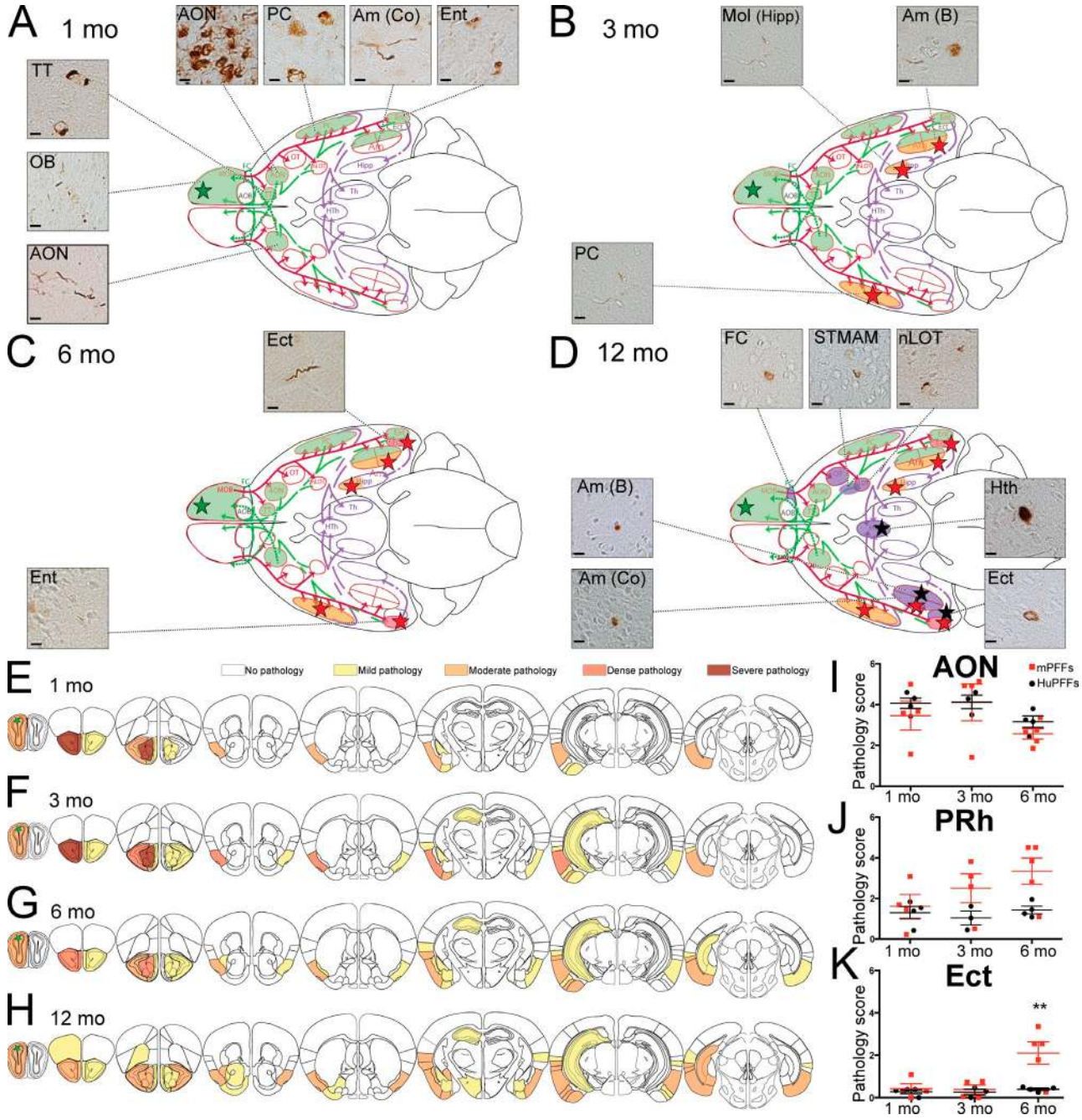

Figure 4. **HuPFFs inoculated in OB led to slower progressive spreading of α-syn pathology first to olfactory structures, and then to connected brain.** (A–D) Schematic of a ventral brain view, depicting the localization of pathology (Pser129) at 1, 3, 6, and 12 mo after huPFFs injections. Micrographs show pathology (Pser129) in related brain regions. (A–E) Histochemical analysis was performed on all animals from the 1-, 3-, 6-, and 12-mo survival time points. The sections were immunostained in eight independent histochemical experiments. 1 and 3 mo delay, $n = 4$ mice per group; 6 and 12 mo delay, $n = 5$ mice per group. (A) At 1 mo delay, pathology was observed in olfactory regions (Ipsi AON, Pc, Am Co, Ent, TT, OB, and contra AON). Bar, 10 µm. (B) At 3 mo delay, pathology appeared in a few more ipsilateral (Mol and Am B) and contralateral brain regions (PC). Regions located one synapse away from the olfactory system are identified with a red star. (C) Pathology appeared in two additional brain regions after 6 mo. (D) 12 mo after injection, additional brain regions show pathology; Regions located 2 synapses away from the olfactory system are identified with black stars. (E–H) Diagram illustrating the anatomical pattern of α-syn pathology in the brain on coronal sections, 1 mo (E), 3 mo (F), 6 mo (G), and 12 mo (H) after injection. (I–K) Scoring of Pser129 immunoreactivity (neurites and cell bodies) in the AON (I), the perirhinal (PRh; J), and ectorhinal cortex (Ect; K). Scoring was performed on all animals from the 1-, 3-, 6-months survival time points. Sections were immunostained in eight independent histochemical experiments (1 and 3 mo delay, $n = 4$ mice per group; 6 mo delay, $n = 5$ mice per group) and were analyzed by two-way ANOVA, followed by a Tukey post-hoc test. Statistics are provided in Table S4. **, $P < 0.05$.

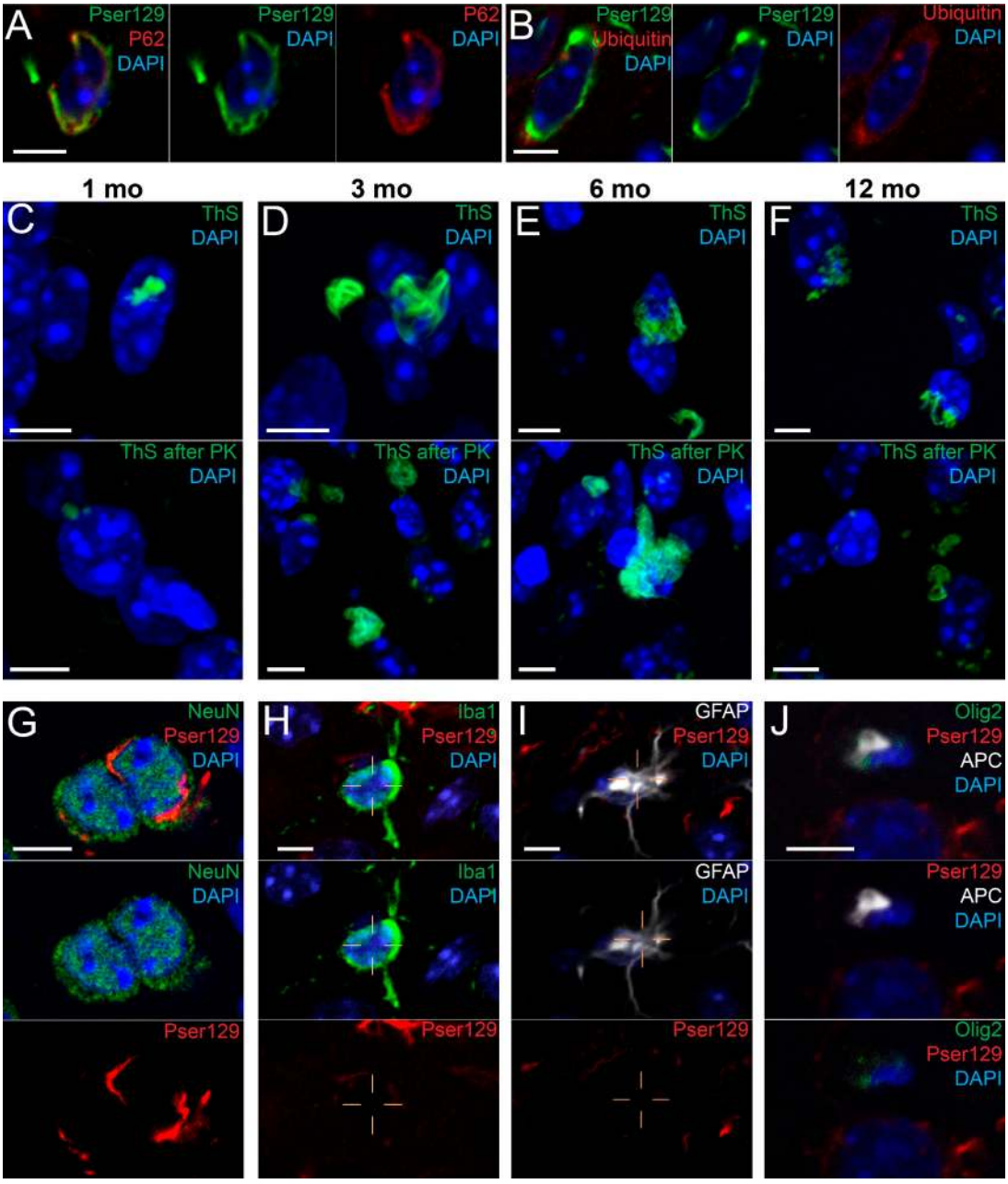

Figure 5. **Inclusions induced by inoculation of mPFFs are positive for markers of Lewy bodies and are present only in neurons.** (A–D) Pser129-positive inclusions (green; DAPI in blue) co-localized with p62 (A, red) and ubiquitin (B, red). Inclusions in the AON are also detected by ThS 1 (C), 3 (D), 6 (E), and 12 mo after injection (C–F) and are resistant to Proteinase K treatment (C–F, bottom). (G–J) Pser129-positive inclusions were detected in NeuN-positive cells (neurons; G), but not in Iba-1– (microglial cells; H), GFAP- (astrocytes; I), or Olig2-APC-CC1–positive cells (oligodendrocytes; J) in the AON, 1 mo after injection. Histochemical analysis was performed on all animals from 1 mo delay (A–B and G–J), and all animals from the 1-, 3-, 6-, and 12-mo survival time points (C–F). The sections were immunostained in one single histochemical experiment for each marker used. 1 and 3 mo delay, $n = 4$ mice per group; 6 and 12 mo delay, $n = 5$ mice per group). Bars: (A–J) 5 µm.

Alternatively, the delayed apparition of inclusions in the OT could be explained by the direction of spreading: If the propagation occurs only retrogradely, then the propagation to the OT would involve indirect connections because the OT does not project back to the OB as opposed to other olfactory regions, and thus propagation to the OT might be slower. After 12 mo, we observed pathology in >40 different brain regions and subregions. Notably, cortical associative and secondary cortical brain regions exhibited pathology, akin to the late appearance of Lewy pathology in the same brain regions

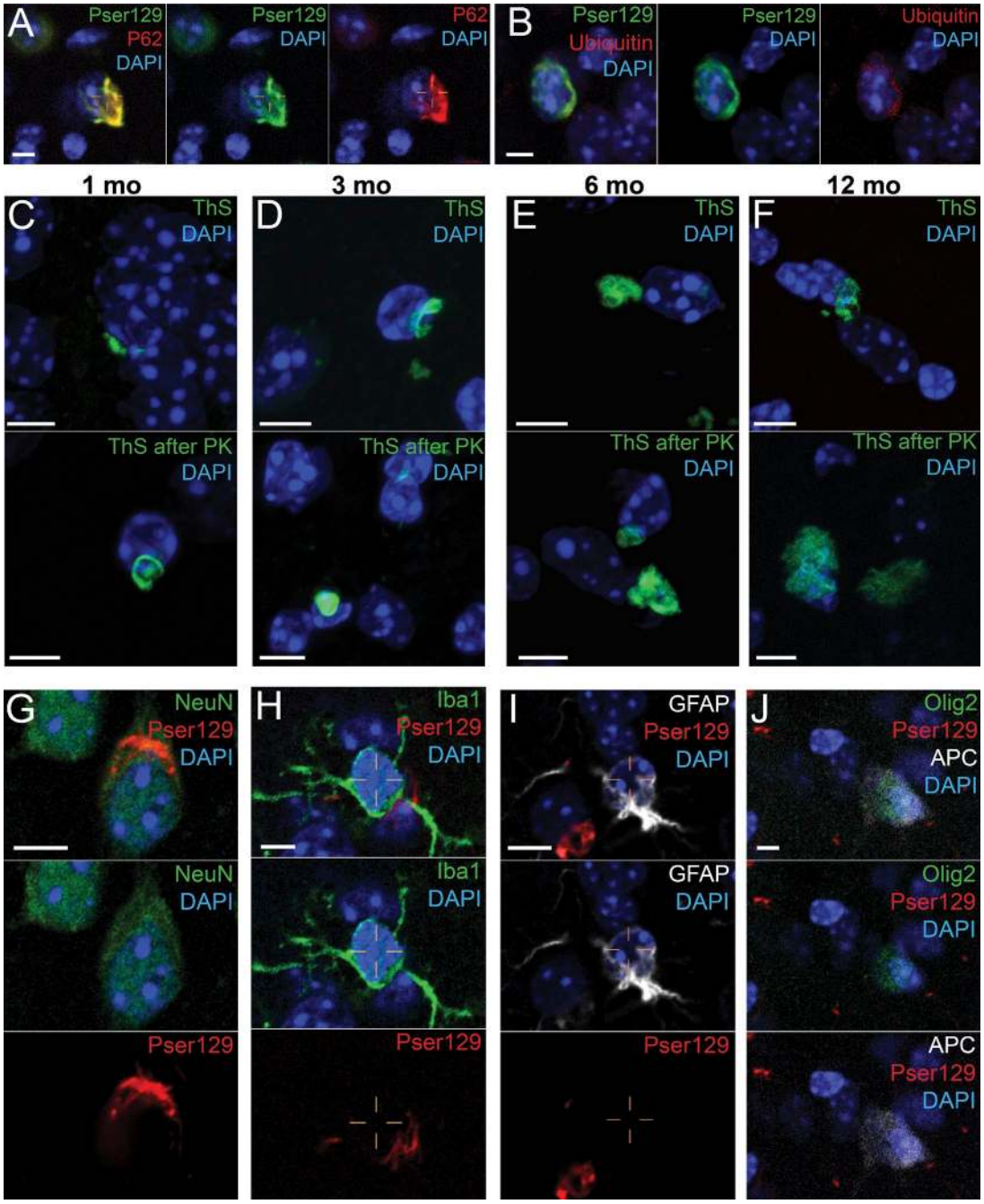

Figure 6. **Inclusions induced by inoculation of HuPFFs are positive for markers of Lewy bodies, and are present only in neurons.** (A–D) Pser129-positive inclusions (green) in AON co-localize with p62 (A, red) and Ubiquitin (B, red). Inclusions in the AON are also ThS positive 1 (C), 3 (D), 6 (E), and 12 mo (F) after injection, and are resistant to Proteinase K treatment (C–F, bottom). (E–H) Pser129-positive inclusions were present in NeuN-positive cells (neurons, E), but not in Iba-1– (microglial cells, F), GFAP- (astrocytes, G), or Olig2-APC-CC1–positive cells (oligodendrocytes, H) in the AON 1 mo after injection. Histochemical analysis was performed on all animals from 1 mo delay (A–B and G–J), and all animals from the 1-, 3-, 6-, and 12-mo survival time points (C–F). The sections were immunostained in one single histochemical experiment for each marker used (1 and 3 mo delay, $n = 4$ mice per group; 6 and 12 mo delay, $n = 5$ mice per group). Bars: (A–J) 5 µm.

in PD according to Braak (stages 4–5) and the unified staging system for Lewy body disorders (Braak et al., 2004; Beach et al., 2009). We also observed Pser129 α-syn–immunoreactive profiles occasionally in the LC, the SN, and the RN at 12 mo after injection of PFFs into the OB. At Braak stage 2 of PD, Lewy pathology appears in the LC, RN, and progresses to the

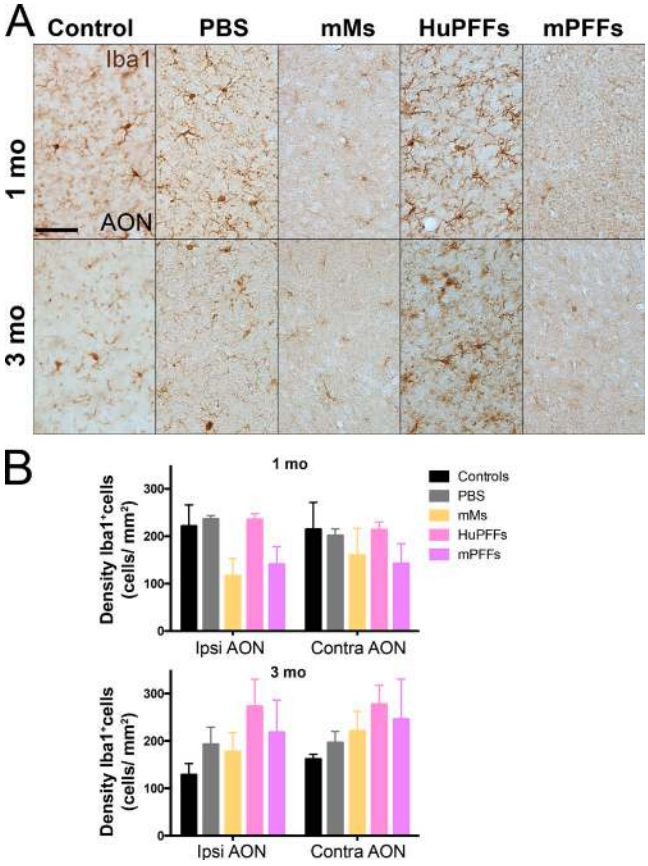

Figure 7. **Changes in the density of microglia after injections of mMs and mPFFs.** (A) Microphotographs of Iba-1–immunopositive cells in the anterior olfactory nucleus (AON) of mice injected with PBS, HuPFFs, mMs, and mPFFs at 1 and 3 mo after injection. The data shown are from one representative animal. Bar, 50 µm. (B) Density of Iba1-positive cells (microglia) in the AON at 1 and 3 mo after injection (n = 4–5 animals per group). Histochemical analysis was performed on all animals from 1- and 3-mo survival time points, in two separate histochemical experiments. Data were analyzed by Linear Mixed-effect Model. After multiple testing corrections, no difference between groups was detected. $P > 0.05$.

SN at stage 3 (Del Tredici and Braak, 2000). Both SN and LC exhibit neuronal death in PD, with it being particularly extensive and functionally detrimental in the SN. Approximately 40% of noradrenergic neurons located in the LC project to the OB (Doty, 2003); 0.5% of neurons from the RN and 3% of nigral dopamine neurons project to the OB in rats (Doty, 2003; Höglinger et al., 2015). It is not clear whether this α-syn pathology was a result of direct transport of α-syn seeds from the injected OB, or from propagation over several synapses, which would explain the long delay (12 mo). However, at this final time point, as a result of the complexity of axonal connections, it is impossible to ascertain precisely which neural connections mediated the spreading of α-syn pathology. Interestingly, although the DMX is postulated to be one of the first brain regions affected by Lewy pathology in PD, we found no Pser129 α-syn immunoreactivity there. These results are consistent with the debated concept that Lewy pathology in the DMX in prodromal PD is triggered by retrograde transport (along the vagal nerve) of α-syn aggregates that were initially formed in the intestinal wall.

In summary, from 1 to 12 mo after injection, we observed a sequential spreading of pathology, first to regions that are directly connected to the OB, and then to structures up to two synaptic connections away from the olfactory system in the ipsilateral hemisphere. Spreading occurs also to the contralateral hemisphere, first to the contralateral AON, directly connected to the ipsilateral OB, and then to structures one and two synapses away from the contralateral AON. We also observed a progressive increase in pathology in regions that were affected early.

Differential effect of mPFFs versus huPFFs injection on the extent of pathology

We also investigated the pathology induced by HuPFFs, which appears to be not as extensive as that of mPFFs. One explanation could be that the pathology triggered by the HuPFFs spread more slowly and to a lesser extent than that produced by mPFFs. Alternatively, differential levels of PFF toxicity could affect the spreading of the two types of injected protein. An earlier study demonstrated that propagation of induced α-syn pathology in the brainstem is reduced when neuronal death occurs and the circuitry is interrupted (Ulusoy et al., 2015). Additionally, in prion biology, partial and complete species barriers can exist when a disease-related protein is transferred between different hosts (Bruce et al., 1994). The amino acid sequences of mouse and human α-syn differ at 7 of the 140 residues (Lavedan, 1998), which might cause differences in fibril structure even after sonication, and in the association of α-syn with other cellular components. Therefore, the transmissibility of the recombinant human α-syn fibrils might be reduced in mouse brain.

Long-term propagation of α-syn pathology and short-term transfer of α-syn from the OB

We previously reported that monomeric and oligomeric human α-syn injected into the mouse OB is transported within a few hours along axonal pathways to the AON, the PC, OT, and amygdala (Rey et al., 2013); those forms of α-syn are cleared from the brain within a few days of injection. In that study, we also found that preparations of pure elongated α-syn fibrils are rarely taken up by mitral cells and consequently are not transported to a great extent to other brain regions. In the present study, α-syn PFFs were subjected to vigorous sonication before injection, resulting in a mixture of α-syn fibrils of varying sizes (Luk et al., 2009;Volpicelli-Daley et al., 2014). Similar preparations injected into mouse or rat striatum trigger pathological intraneuronal α-syn accumulation in nigral dopamine neurons and subsequent degeneration of a subset of these neurons (Luk et al., 2012a; Paumier et al., 2015). Based on our own observations, we suggest that the differences in outcome after injection of pure elongated

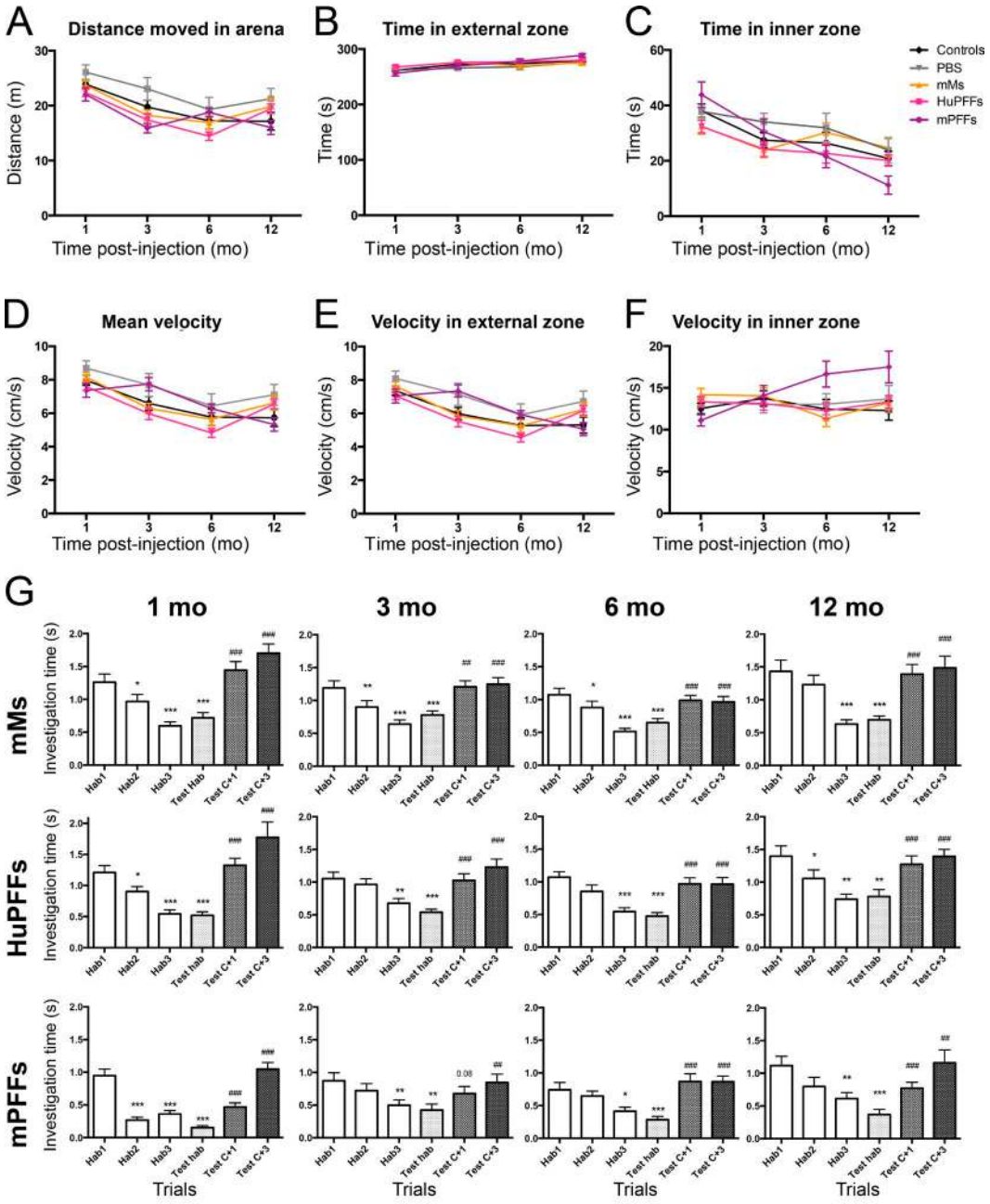

Figure 8. **mPFFs- and HuPFFs-injected mice did not exhibit alteration of locomotion or anxiety level, or deficits in odor discrimination in the open field test.** (A) Total distance moved in the area during a 5-min trial. (B and C) Time spent in external zone (B) and in inner zone (C). (D) Mean velocity in the open field. (E–F) Velocity of mice in the external zone (E) and the inner zone (F). Behavioral data were acquired from four independent experiments. No significant differences ($P > 0.05$; analysis by linear mixed-effect models) were observed between groups and across aging. Number of animals per group (control, mMs, PBS, HuPFFs, and mPFFs, respectively) for 1-mo survival time point: 25, 29, 44, 43, and 33; 3-mo survival time point: 21, 25, 39, 39, and 28; 6-mo survival time point: 18, 17, 32, 36, and 28; and 12-mo survival time point: 11, 9, 29, 25, and 17. (G) Odor discrimination test. Mice were first habituated during a prehabituation trial with MO. Next, mice were exposed to the habituation odor during three successive trials (OHab1, OHab2, and OHab3) and, finally, to three presentations of test odorants (Test OHab, Test C+1, Test C+3) in a random order, separated by a presentation of habituation odor (OHab) between each test odorant. All the mice habituated to the habituation odor during the three first trials and investigated the odors C+1 and C+3 more significantly during the discrimination phase, indicating that they discriminated C+1 and C+3 odorants from the odor of habituation. Thus, no group exhibited a deficit in discrimination at any time point. Behavioral data were acquired from four independent experiments. Numbers of animals per group (control, mMs, PBS, HuPFFs, and mPFFs, respectively) for 1-mo survival time point: 22, 26, 40, 37, and 29; 3-mo survival time point: 16, 21, 33, 35, and 23; 6-mo

α-syn fibrils or α-syn PFFs is that the latter contain shorter fibrils that are readily taken up by neurons and transported along axons within a short timeframe, seeding endogenous α-syn rapidly for further aggregation and propagation.

Similarities and differences between PFFs-induced α-syn pathology and Lewy pathology in PD

The Pser129-positive inclusions induced by PFFs injections co-localized with molecular markers typically used to evaluate Lewy pathology in human disease. Inclusions were hyperphosphorylated on ser129, resistant to proteinase K and co-localized with p62 and ubiquitin, similar to Lewy bodies found in PD, but their morphology differed from that of Lewy bodies. PFFs-induced inclusions had a tendril-like cytoplasmic structure that wrapped around the nucleus, similar to those observed in a previous study (Osterberg et al., 2015). The Pser129-positive structures were also larger than and morphologically different from the ThS-stained inclusions observed in the same mice. We speculate that the α-syn aggregates consist of a mature, insoluble amyloid ThS-positive core surrounded by a less compact α-syn that is ThS negative, but Pser129, p62, and ubiquitin positive. Notably, we detected inclusions only in neurons, not in astrocytes, oligodendrocytes, or microglia. The absence of α-syn aggregates in glia suggests that propagation between brain regions was not due to release of α-syn seeds from migrating astrocytes or microglia, but more likely transneuronal propagation after axonal transport of the α-syn seeds.

Progressive olfactory deficit accompanying progression of α-syn pathology

We monitored the mice injected with PFFs in multiple behavioral paradigms. Importantly, the propagation of α-syn pathology throughout the brain was accompanied by progressive and specific deterioration of olfactory function, similar to the olfactory deficits seen in early PD, even during the prodromal phase before the emergence of motor deficits (Kranick and Duda, 2008; Haehner et al., 2009). Although odor detection and odor retention were severely impaired, no deficits in odor discrimination, and no alteration of locomotion or anxiety in open field testing were observed. Importantly, the PFFs were injected unilaterally into 1 OB. Related mechanical damage should not affect sense of olfaction because unilateral bulbectomy does not alter olfactory function in rodents (Slotnick et al., 1987). Further, control mice injected with vehicle or α-syn monomers showed no deficits; and no loss of mitral cells was detected in the OB in either of the groups injected with PFFs. This suggests that deficits we observed are unlikely to be the result of mechanical damage or neuronal loss in the OB itself.

The lack of deficits in olfactory discrimination might be explained by the relative lack of α-syn pathology in the OT, which is known to play an important role in this faculty (Wesson and Wilson, 2011). Notably, odor detection relies on the processing of olfactory input by the OB, which enhances the sensitivity of odors by lateral inhibition mechanisms (Wilson and Leon, 1987).

Pathology was less severe in the PC, OB, and OT of mice injected with HuPFFs than mPFFs, which is consistent with the olfaction deficits being less severe in the mice injected with HuPFFs. Furthermore, spreading of α-syn pathology to the contralateral hemisphere was less pronounced in the mice injected with HuPFFs, opening up the possibility that spared contralateral structures might have compensated for functional changes in the ipsilateral hemisphere.

Concluding remarks

In conclusion, we provide the first evidence of a transneuronal, progressive propagation of PD-like α-syn pathology from the OB to central brain regions, accompanied by specific and progressive deficits in olfactory function. Hence, our model of α-syn propagation is highly relevant to prodromal PD. It also supports the idea that the OB could be a starting point of α-syn pathology from which it spreads to other olfactory structures and the basal ganglia, as well as neocortical regions. The neuropathology (at both molecular and anatomical levels), as well as the functional deficits, are faithful to observations made in prodromal and manifest PD, and that the rate of progression is slow over several months should make this model of α-synucleinopathy powerful when testing novel therapies aimed at modifying disease progression.

MATERIALS AND METHODS

Animals

We purchased C57BL/6J 3-mo-old female mice from Charles River laboratories and the Jackson Laboratory and housed them five to six per cage under a 12-h light/12-h dark cycle with access to food and water ad libitum. The housing of the animals and all procedures were in accordance with the European international guidelines, with the Guide for the Care and Use of Laboratory animals (United States National Institutes of Health) and were approved by the Malmö-Lund ethical Committee for Animal research and Van Andel Research Institute's institutional animal care and use committee guidelines.

Stereotactic injections

Purification of recombinant full-length mouse α-syn and full-length human α-syn and fibril assembly were performed as previously described (Volpicelli-Daley et al., 2014). Before

survival time point: 18, 19, 36, 35, and 21; and 12-mo survival time point: 8, 7, 27, 23, and 14. Habituation and discrimination were analyzed by one-way ANOVA with repeated measures. We then performed multiple comparisons by a Sidak post-hoc test. *, P = 0.05; **, P = 0.01; ***, P = 0.001 for difference from Hab1. ##, P = 0.01; ###, P = 0.001 for difference from Test Hab. Results of the ANOVAs and number of animals per group are provided in Table S4.

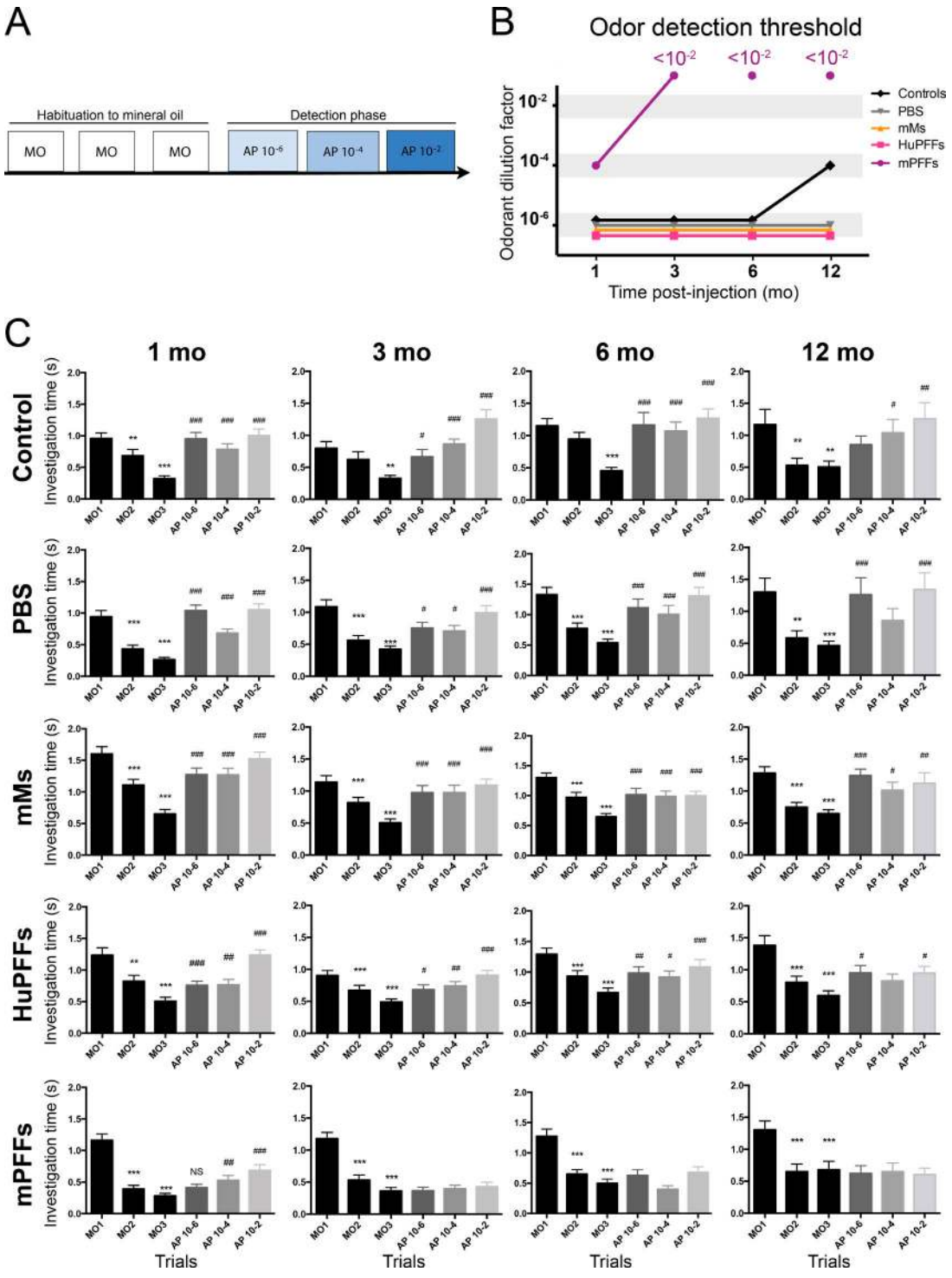

Figure 9. **PFFs–injected mice exhibit a progressive alteration of odor detection.** (A) Experimental design of the odor detection test. Mice were exposed to MO for three consecutive trials (habituation), and then to increased concentrations of propionic acid (AP; dilution factor, 10^{-6}, 10^{-4}, or 10^{-2}) during three other trials. (B) Summary of the results of the odor detection test. Dots represent the odorant threshold detected (measured as the dilution factor used), for each animal group at 1, 3, 6, and 12 mo after injection. Whereas control-, PBS-, mMs-, and HuPFFs-injected mice show a low odor threshold (10^{-2}) from 1 to 6 mo after injection; mice injected with mPFFs exhibit a strong deficit of odor detection appearing at 3 mo, with an odor detection threshold higher than the 10^{-2} dilution. (C) Odor detection results. All mice display habituation across the trials with the odor of habituation (OHab). Control, PBS-, mMs-, and HuPFFs-injected mice investigate significantly more the odorant at the lowest concentration compared with OHab, demonstrating that their odor detection threshold is 10^{-6}. The mice injected with mPFFs show a mild deficit of odor retention already at 1 mo after injection. At 3 mo after injection,

injections, the PFFs were thawed and sonicated at room temperature by probe sonication (QSonica; 15% power, for 10 pulses of 0.5 s ON, 1 s OFF, repeated four times with 5-min intervals). Recombinant soluble mouse α-syn was thawed and kept on ice during the surgical procedures.

We anesthetized 202 mice (3 mo old) with isoflurane/oxygen mixture, and stereotactically injected sterile PBS, mouse monomers (mMs), WT mouse α-syn PFFs (mPFFs) or WT human α-syn preformed fibrils (HuPFFs) into the OB. We performed the stereotactic injections using a glass capillary attached to a 10 µl Hamilton microsyringe, and injected 0.8 µl of protein (5 µg/µl in sterile PBS) or PBS unilaterally in the OB (coordinates: AP, +5.4 mm; L, −0.75 mm; DV, −1 mm relative to bregma and dural surface) at a constant rate of 0.2 µl per minute as previously described (Rey et al., 2013). The capillary was left in place for 4 min after injection, and then slowly removed.

Preparation of the tissue

We perfused the mice at various time points (1.5 h, 1 mo, 3 mo, 6 mo, and 12 mo after injection). We anesthetized mice with sodium pentobarbital and perfused them transcardially with 0.9% saline, followed by 4% PFA in phosphate buffer. We collected the brains (4–5 mice per group) for histology, post-fixed them for 24 h in 4% PFA, and placed them in 30% sucrose in phosphate buffer. We stored the brains at 4°C until sectioning. We cut the entire brain of each mouse into 30-µm free-floating coronal sections on a freezing microtome, and stored them in antifreeze solution at 4°C until immunostaining.

Immunohistochemistry

We stained coronal free-floating sections using primary antibodies and secondary biotinylated antibodies listed in Table S5. For the detection of the antibody with DAB, we used a standard peroxidase-based method (Vectastain ABC kit and DAB kit; Vector Laboratories). Sections stained for human α-syn were then counterstained by hematoxylin. After dehydration, slides are coverslipped with Cytoseal 60 mounting medium (Thermo Fisher Scientific). We analyzed sections with conventional light using an Eclipse Ni-U microscope (Nikon); images were captured with a Retiga 2000R digital camera using NIS Elements AR 4.00.08 software (Nikon).

For analysis of pathology spreading in the brains of mice, we stained with anti-pser129 antibody a whole series of coronal sections (210-µm intervals between consecutive sections) from four to five animals per group (noninjected, PBS, mMs, mPFFs, and HuPFFs injected groups). We assessed in a blinded manner the presence of pser129-positive accumulations by screening every single section at 20× magnification using an Eclipse Ni-U microscope (Nikon).

Immunofluorescence staining

We stained coronal free-floating sections with primary antibodies and appropriate secondary antibodies listed in Table S5.

The sections to be stained with ThS were first mounted on glass slides and then rehydrated in PBS. Sections were then incubated for 8 min at room temperature with 0.05% ThS that had been diluted into distilled water and filtered. Sections were then differentiated for 3 min in 80, 95, and then 95% ethanol, and treated with TrueBlack (Biotium) at a 1:20 concentration in 70% ethanol for 30 s, washed in PBS, and mounted with EverBrite mounting medium (Biotium).

We analyzed blind coded sections with an inverted confocal laser microscope Nikon Eclipse Ti-E (Nikon). To acquired images we applied a median filter (kernel 3) to remove noise. All images were generated using NIS Elements AR 4.00.08 software (Nikon).

Scoring of pathology

On blind coded sections, we assessed the accumulation of α-syn pathology (pser129-positivity) in selected brain structures (AON, perirhinal [PRh], and ectorhinal [Ect] cortices) in animals that were 1, 3, and 6 mo after injection (four to five animals per group) by scoring cell bodies and neurites positive for phosphorylated α-syn (Pser129). We first set a scoring scale from 1 to 5 specific for each single brain region using template images (0, no aggregates; 1, sparse [very few neurites, max 1 soma]; 2, mild [more neurites, with or without soma]; 3, moderate [many soma and neurites, but large areas without aggregates]; 4, dense; 5, very dense). Next, we assigned a score to each section and brain region (corresponding stereotactic antero-posterior coordinates [from Bregma] as described in Paxinos and Franklin (2012): AON, 3.20–1.98 mm; PRh, −1.34–−4.36 mm; Ect, −1.34–−4.36 mm), by comparison with the template images. We calculated the mean score value for each brain region per animal. We then calculated the mean score values per group, and analyzed them using two-way unpaired ANOVA followed by Tukey post-hoc multiple comparisons on Prism 6.0 (GraphPad Software). Data points represent mean values from each animal score.

all mice except the mPFFs-injected mice detect the lowest concentration (10^{-6}). From this time point, the mPFFs-injected mice exhibit a severe alteration of odor detection (unable to detect the higher concentration used here). The mean exploration time per trial was analyzed by one-way ANOVA with repeated measures across trials for each group and time point. Results of the ANOVAs are provided in Table S4. Behavioral data were acquired from four independent experiments. Number of animals per group (control, PBS, mMs, HuPFFs, and mPFFs, respectively) for 1-mo survival time point: 22, 26, 40, 37, and 29; 3-mo survival time point: 16, 21, 33, 35, and 23; 6-mo survival time point: 18, 19, 36, 35, and 21; and 12-mo survival time point: 8, 7, 27, 23, and 14. We then performed multiple comparisons by Sidak post-hoc tests (more conservative than Fisher LSD post-hoc test). *, P = 0.05; **, P = 0.01; ***, P = 0.001 for difference from MO1. #, P = 0.05; ##, P = 0.01; ###, P = 0.001 for difference from MO3.

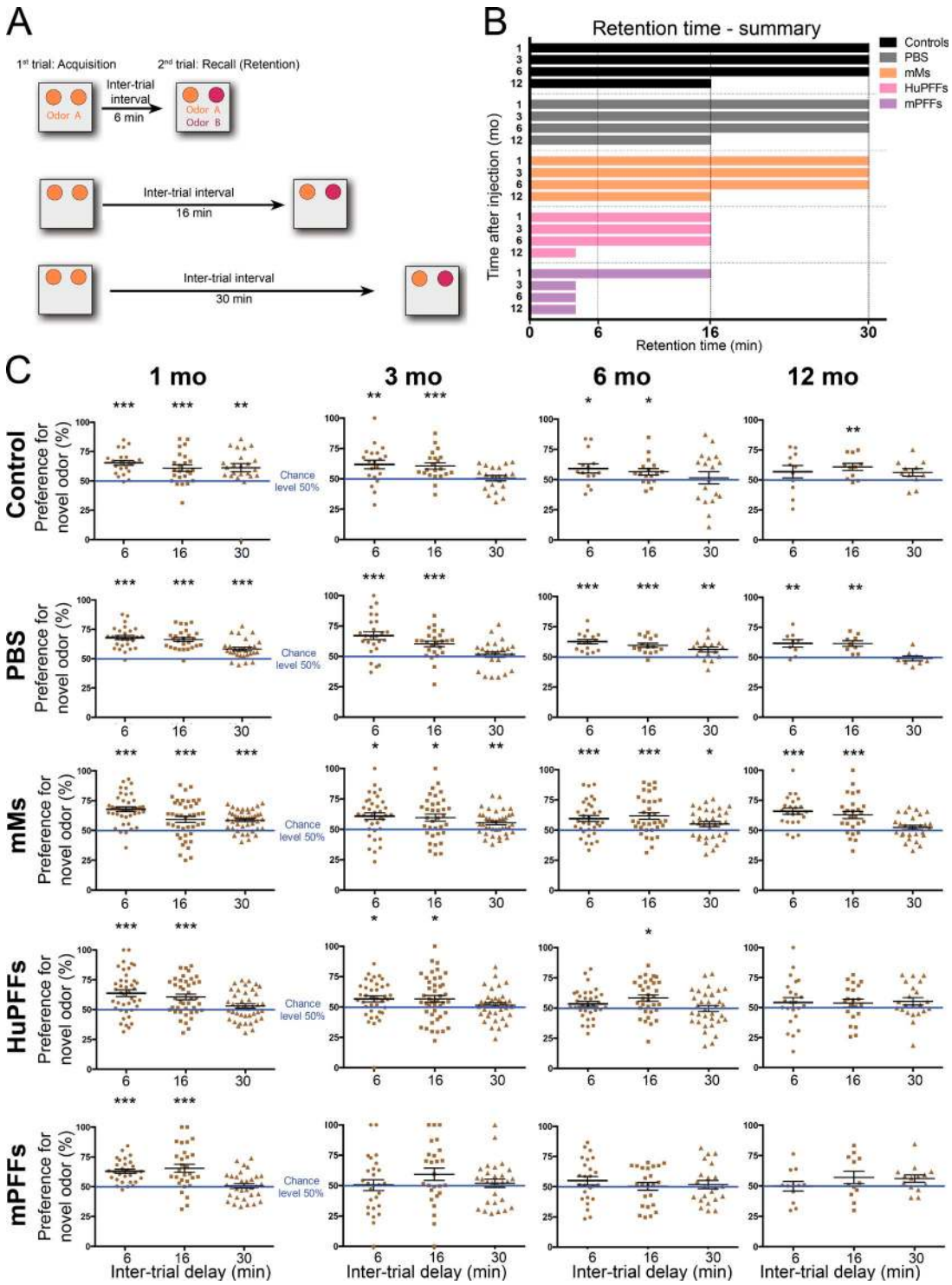

Figure 10. **Mice injected with PFFs develop a progressive alteration of odor retention.** (A) Experimental design of the odor retention test. During the first trial (acquisition), mice were exposed to the same odor in two cartridges. After a delay of 6, 16, or 30 min, mice were exposed to the first odor (familiar odor) in one cartridge, and a new scent (novel odor) in the second cartridge during a second trial (recall). (B) Summary of the results of the odor retention test. Bar lengths represent the median duration of odor retention for each group. Control, PBS, and mMs groups show a slight decrease of retention time at 12 mo, which is an effect of normal aging. HuPFFs mice show a deficit of retention at 1 mo, which remains steady until it is exacerbated after 12 mo. mPFFs mice show severe shortening of odor retention already after 3 mo. (C) Odor retention results. Results are expressed as a preference for novel odor versus the familiar odor, at the 3 time points used. mMs mice display a preference for the novel odor above the chance level of 50% at 6, 16, and 30 min inter-trial

Mitral cell density

To measure the density of mitral cells in the OB, we stained sections with Cresyl violet (one section every eighth section). Slides were incubated for 9 min in 0.1% Cresyl violet solution, and were dipped into 95%, 100% ethanol and xylene before coverslipping with Cytoseal 60 mounting medium (Thermo Fisher Scientific). On blind coded sections stained with Cresyl violet, we measured the density of mitral cells in the mitral cell layer of the OB. Mitral cells can be easily identified from other cells based on their morphology (large nucleus and cytoplasm). Quantifications were done on a computer-assisted mapping and cell quantification program (Stereo Investigator; MBF Bioscience) coupled to an Imager M2 microscope (ZEISS). We analyzed four sections per animal spaced by 450 µm, and distributed along the rostrocaudal axis at equivalent locations in each animal, in four to five animals per group. We outlined the mitral cell layer and counted every mitral cell in that area. We then calculated the density of cells per section (number of cells per surface area) and the mean density per animal. We then calculated the mean density per group and analyzed the data by Kruskal–Wallis testing with post-hoc Dunn's multiple comparison analysis using Prism 6.0 (GraphPad Software).

Iba1-positive cells density

On blind coded sections, we measured the density of Iba1-positive cells in the AON (diaminobenzidine stained) using a computer-assisted mapping and cell quantification program (Stereo Investigator; MBF Bioscience) coupled to a NIKON Eclipse Ni-U microscope (Nikon). We analyzed three sections per animal spaced by 450 µm, and distributed along the rostrocaudal axis at equivalent locations in each animal, in four to five animals per group. We outlined the AON and counted every positive cell in each section. We then calculated the density of cells per section (number of cells per surface area) and calculated the mean density per animal. We then calculated the mean density per group and analyzed the data with linear mixed-effects models (LMMs) with the software R. We included a random intercept for mouse to account for the fact that we measured densities on both sides of the brain in each animal, and we stratified the analysis by time. Time, group, and side (ipsilateral and contralateral side to injection) were included as covariates. Tests for differences between groups were done using linear contrasts and false discovery rate correction. After multiple testing corrections, no difference between groups was detected. However, some effects were significant before this correction (Controls/mMs; Controls/mPFFs), suggesting that there might exist true effects and that, as a result of inter-animal variability within groups, the study was not sufficient to detect them.

Open field test

To evaluate general locomotor activity and anxiety, mice were tested in an open field arena for one trial at 1, 3, 6, and 12 mo in a blinded manner. A square arena (48 cm × 48 cm × 35 cm) with white background was used and illuminated evenly. Mice were habituated to the arena the day before the test. During the test, mice were placed in the arena for 5 min, and their activity was recorded and analyzed by videotracking system ANYmaze (Stoelting). We assessed the total distance traveled, the mean speed, the velocity, and the time spent in an inner centered zone (24 cm × 24 cm) and in the external zone.

We analyzed the total distance traveled, the mean speed, the velocity, and the time spent in an inner centered zone and in the external zone. The differences between groups and over time, and their interaction were analyzed with multiple LMMs with the software R. LMMs appropriately adjust for repeated measures and allow missing values (animals sacrificed at previous time points), unlike repeated measure ANOVA. LMMs can also adjust for a portion of the within-subject variation via random slopes and intercepts. Both of these features should result in superior model performance and accuracy (Krueger and Tian, 2004). Each model was fit, including random intercepts, to account for the high variability in mice at the initial time point. Final models included time and experimental group main effects, as well as interactions between both factors. When interactions were nonsignificant, they were abandoned and the models were refit. All the parameters except "Time in external zone" were analyzed using quadratic term (based on Akaike and Bayesian information criteria). Within each outcome, we compared each treatment group to all others using contrasts and Tukey's honest significant difference to correct for multiple testing. All outliers (residuals more than three standards deviation away from mean residual) were inspected for possible recording errors or extreme experimental issues. We found no convincing reasons to remove any of these mice. Normality and homoscedasticity were checked using quantile–quantile plots and residual plots.

delays, indicating that the mice could remember the familiar odorant for at least 30 min (retention time) at any time point. HuPFFs and mPFFs mice exhibit a retention time of only 16 min 1 mo after injection. mPFFs mice show a decrease in retention time (<6 min) 3 mo after injection, whereas HuPFFs mice show a further alteration of retention (to <6 min) only 12 mo after injection. Notably, after 3 mo, control and PBS groups show transient inability to recall the novel odor after 30 min, whereas groups injected with mMs perform well. This is probably a result of the relatively small sample sizes in the control and PBS groups. Behavioral data were acquired from four independent experiments. Number of animals per group (control, PBS, mMs, HuPFFs, and mPFFs, respectively) for 1-mo survival time: 22–24, 25–29, 40–42, 41, and 29–32; 3-mo survival time point: 20–21, 25, 36–39, 36–43, and 26–28; 6-mo survival time point: 15–18, 15–16, 33–34, 33–34, and 22–25; and 12-mo survival time point: 11, 8–9, 22–28, 21–23, and 12–14 (numbers vary depending on which retention delay is tested). Mean preference for the novel odor for each group during the recall trial was analyzed by one-sample Student's *t* test compared with the chance level of 50% *, $P < 0.05$; **, $P < 0.01$; ***, $P < 0.001$.

Odor detection test

We tested the detection threshold of the odorant propionic acid (AP) in mice using three different concentrations of the odorant: 10^{-6}, 10^{-4}, and 10^{-2} in mineral oil (MO). For all olfactory tests, the odorants were diluted the day before the test in MO, and tests were performed at 1, 3, 6, and 12 mo after injection, with 25–30 mice per group by a blinded experimenter.

The detection test was performed in clean cages without bedding, and in a blinded manner. A paper swab was impregnated with the odorant and placed in a mesh ball hanging in the cage. We first habituated the mice to the setting during a prehabituation trial with MO. Mice were then exposed to MO for three trials of 50 s with a 5-min interval (habituation phase, MO), and then exposed during three consecutive trials to increasing concentrations of the odorant (AP 10^{-6}, AP 10^{-4}, and AP 10^{-2}; Fig. 6 a). During each trial, we recorded investigation time as defined as the duration of active sniffing with the nose placed less than 1 cm from the mesh ball. Mice that did not investigate the MO during the first habituation trial were excluded, and outliers defined by an investigation time higher than the mean + 2 SD were also excluded. We calculated the mean exploration time per trial and analyzed the data by one-way ANOVA with repeated measures across trials for each group and time point, first for the habituation phase (MO1, MO2, and MO3), which is critical for being able to interpret the results from the following detection phase, and then for the detection phase (MO3, AP 10^{-6}, AP 10^{-4}, and AP 10^{-2}), followed by Sidak post-hoc test (more conservative than Fisher LSD post-hoc test) to compare MO1 to MO2, MO3, and MO3 to AP 10^{-6}, AP 10^{-4}, and AP 10^{-2} using Prism 6.0 (GraphPad Software).

Odor discrimination test (habituation/discrimination)

This test assesses habituation and discrimination in a nonassociative memory task. We used cross-habituation between a structurally and perceptually similar odorant to measure nonassociative odor memory (Cleland et al., 2002; Rey et al., 2012a,b). Odorants used in this test (sets of acetate esters and aldehydes) were used at a vapor phase partial pressure of 1Pa (Rey et al., 2012a,b). Within a set of odorants, odorants were from a same chemical family but differed by the length of their carbon chain, which define in a correlated manner their perceptual proximity (Cleland et al., 2002). Similar to the detection test, the odorant was placed in a mesh ball, and mice were exposed to MO during a prehabituation trial (Fig. 6 b), and the test was performed in a blinded manner. Next, mice were exposed to the habituation odorant (OHab1, OHab2, and OHab3; habituation phase) during three consecutive trials (50 s duration, 5-min interval), followed by three randomized presentations of the test odorants (Test OHab, Test C+1, and Test C+3; detection phase) separated by a presentation of habituation odor (OHab) between each test odor. Investigation time is recorded for each trial of habituation and discrimination phases. Mice that did not investigate the OHab during the first habituation trial, and outliers, are defined by an investigation time higher than the mean +2 standard deviations were excluded. We calculated the mean investigation time for each trial within each group, and habituation and discrimination were analyzed by one-way ANOVA with repeated measures, first for the habituation phase (OHab1, OHab2, OHab3, and Test OHab), which is critical for being able to interpret the results from the following discrimination phase, and then for the discrimination phase (Test OHab, C+1, and C+3; Rey et al., 2012a). We then performed multiple comparisons by Sidak post-hoc test (more conservative than Fisher LSD post-hoc test) to compare OHab1 to OHab2, OHab3, and Test OHab; and to compare OHab to C+1 and C+3 using Prism 6.0 (GraphPad).

Odor retention test (odor recognition task)

This test assessed short-term olfactory memory in a two-trial odor recognition task, using pairs of odorants. The protocol was adapted from previous work (Mandairon et al., 2009; Rey et al., 2012a,b). Before the first test, mice were prehabituated to the setup for 5 min with empty cartridges in the test cage. During the test (performed in a blinded manner), mice were exposed to two odorants at a time and placed in cartridges containing a paper swab. During the first trial (Acquisition), mice were exposed to the same unfamiliar odorant in the two cartridges. After 6, 16, or 30 min, mice were exposed during a second trial (Recall) to a cartridge containing the same odorant at the first trial, and a second cartridge with a novel odorant (Fig. 6 C). We recorded odorant investigation (defined as in the previous tests), and calculated the preference of the mouse for the novel odor during the recall trial. We chose three pairs of odorants (familiar and novel odor) used at supraliminal concentration, and known for having equal hedonicity among each pair (Rey et al., 2012a,b): (-) limonene (diluted 1:10) and (+) carvone (diluted 1:10); Amylacetate (1:100) and Anisol (1:100); and propyl acetate (1:10) and Pentanal (1:10). The use of each odorant from the pair as familiar or novel odor is randomized. Mice that did not investigate the odorants during the acquisition trial, and outliers defined by an investigation time higher than the mean +2 standard deviations were excluded. Data are expressed as a preference for novel odor. The mean preference for novel odor for each group during the recall trial was analyzed by one-sample Student's *t* test compared with the chance level of 50% (Prism 6.0; GraphPad). The odorants used in the different behavioral tests were purchased from Sigma-Aldrich, TCI America, or provided by A. Didier (Lyon Neuroscience Research Center, Lyon, France).

Online supplemental material

Tables S1 and S2, available as Excel files, summarize the progression of pathology observed after PFFs injection. Table S3, available as an Excel file, contains a list of abbreviations. Table S4, available as an Excel file, gathers additional details on statistical analyses. Table S5, available as an Excel file, is

a list of antibodies used in this study. Online supplemental material is available at http://www.jem.org/cgi/content/full/jem.20160368/DC1.

ACKNOWLEDGMENTS

We thank Emily Schulz, Darcy Marckini, and Marie Persson-Vejgården for their technical assistance; Dr. Sonia George for advice on and expertise with confocal microscopy; Dr. Mary Winn from the Bioinformatics and Biostatistics Core of the Van Andel Research Institute; David Nadziejka from the Van Andel Research Institute, for text editing; the Confocal Core of the Van Andel Research Institute; and the staff of the Vivarium of Van Andel Research Institute and of Lund University for animal care. We are grateful to Dr. Jeffrey Kordower for critical reading of the manuscript, to Dr. Anne Didier for providing some odorants for the behavioral tests, and to Drs. Darren Moore and Peter Davies for providing PHF1 and CP13 antibodies.

We acknowledge the Van Andel Research Institute and the many individuals and corporations that financially supported the neurodegenerative research at Van Andel Research Institute. N.L. Rey is supported by the Peter C. and Emajean Cook Foundation. N. Maroof is supported by a Roche Postdoctoral Fellowship (RPF) grant.

Pilot experiments were supported by the European Research Council (PRISTI NE-PD 269064 to P. Brundin). P. Brundin reports grants from The Michael J. Fox Foundation, National Institutes of Health (NIA PO1 AG 17586-10, PO1 AG-032953, NINDS P50 NS053488-02, and NIA UO1 AG029213-01 to V.M.-Y. Lee), Cure Parkinson's Trust, TEVA Neuroscience, East Tennessee Foundation, KiMe Fund, and Campbell Foundation, which are outside the study but relevant to the submitted work. Additionally, we acknowledge organizational support from the Van Andel Research Institute. K.C. Luk, J.Q. Trojanowski, and V.M.-Y. Lee acknowledge support from the Penn Morris K. Udall Parkinson's Disease Research Center of Excellence (NS53488). V.M.-Y. Lee also received research support from the Marian S. Ware Alzheimer Program.

Dr. Brundin has received commercial support as a consultant from Renovo Neural, Inc., Roche, and Teva Inc, Lundbeck A/S, AbbVie, ClearView Healthcare, FCB Health, IOS Press Partners and Capital Technologies, Inc. Additionally he has received commercial support for grants/research from Renovo and Teva/Lundbeck. Dr. Brundin has ownership interests in Acousort AB and Parkcell AB. Dr. Trojanowski serves as an Associate Editor of Alzheimer's and Dementia. He may accrue revenue on patents submitted by the University of Pennsylvania wherein he is inventor including: Modified avidin-biotin technique, method of stabilizing microtubules to treat Alzheimer's disease, method of detecting abnormally phosphorylated tau, method of screening for Alzheimer's disease or disease associated with the accumulation of paired helical filaments, compositions and methods for producing and using homogeneous neuronal cell transplants, rat comprising straight filaments in its brain, compositions and methods for producing and using homogeneous neuronal cell transplants to treat neurodegenerative disorders and brain and spinal cord injuries, diagnostic methods for Alzheimer's disease by detection of multiple MRNAs, methods and compositions for determining lipid peroxidation levels in oxidant stress syndromes and diseases, compositions and methods for producing and using homogenous neuronal cell transplants, method of identifying, diagnosing and treating α-synuclein–positive neurodegenerative disorders, mutation-specific functional impairments in distinct tau isoforms of hereditary frontotemporal dementia and parkinsonism linked to chromosome-17: genotype predicts phenotype, microtubule stabilizing therapies for neurodegenerative disorders, and treatment of Alzheimer's and related diseases with an antibody. He is co-inventor on patents submitted to the University of Pennsylvania, wherein he is the inventor and has generated income he has received from the sale of Avid to Eli Lily, including amyloid plaque aggregation inhibitors and diagnostic imaging agents.

Dr. Lee has received funding for travel and honoraria from Takeda Pharmaceutical Company Ltd.; has received speaker honoraria from Pfizer Inc., BMS and Merck; may accrue revenue on patents re: Modified avidin-biotin technique, method of stabilizing microtubules to treat Alzheimer's disease, method of detecting abnormally phosphorylated tau, method of screening for Alzheimer's disease or disease associated with the accumulation of paired helical filaments, compositions and methods for producing and using homogeneous neuronal cell transplants, rat comprising straight filaments in its brain, compositions and methods for producing and using homogeneous neuronal cell transplants to treat neurodegenerative disorders and brain and spinal cord injuries, diagnostic methods for Alzheimer's disease by detection of multiple MRNAs, methods and compositions for determining lipid peroxidation levels in oxidant stress syndromes and diseases, compositions and methods for producing and using homogenous neuronal cell transplants, method of identifying, diagnosing and treating alpha-synuclein positive neurodegenerative disorders, mutation-specific functional impairments in distinct tau isoforms of hereditary frontotemporal dementia and parkinsonism linked to chromosome-17: genotype predicts phenotype, microtubule stabilizing therapies for neurodegenerative disorders, and treatment of Alzheimer's and related diseases with an antibody.

The authors declare no additional competing financial interests.

Author contributions: N.L. Rey designed the study; performed the injections, behavioral tests, histology, and analysis and interpretation of behavioral data and histological results; and wrote the manuscript. J.A. Steiner provided critical expertise and contributed to study design, and wrote the manuscript. N. Maroof performed measurements to define densities of microglia. Z. Madaj performed and interpreted the statistical analysis of the open field test and the Iba1-positive cell density by linear mixed-effect models, and wrote related parts of the manuscript. K.C. Luk, J.Q. Trojanowski, and V.M.-Y. Lee synthetized and provided the PFFs for injections, contributed to scientific discussion of the results and discussion on the design of the study, and edited the manuscript. P. Brundin contributed to the design of the study, interpretation of the results, and wrote the manuscript. All authors gave input to the manuscript.

Submitted: 10 March 2016

Accepted: 16 June 2016

REFERENCES

Beach, T.G., C.H. Adler, L. Lue, L.I. Sue, J. Bachalakuri, J. Henry-Watson, J. Sasse, S. Boyer, S. Shirohi, R. Brooks, et al. Arizona Parkinson's Disease Consortium. 2009. Unified staging system for Lewy body disorders: correlation with nigrostriatal degeneration, cognitive impairment and motor dysfunction. *Acta Neuropathol.* 117:613–634. http://dx.doi.org/10.1007/s00401-009-0538-8

Braak, H., K. Del Tredici, U. Rüb, R.A.I. de Vos, E.N.H. Jansen Steur, and E. Braak. 2003a. Staging of brain pathology related to sporadic Parkinson's disease. *Neurobiol. Aging.* 24:197–211. http://dx.doi.org/10.1016/S0197-4580(02)00065-9

Braak, H., U. Rüb, W.P. Gai, and K. Del Tredici. 2003b. Idiopathic Parkinson's disease: possible routes by which vulnerable neuronal types may be subject to neuroinvasion by an unknown pathogen. *J Neural Transm (Vienna).* 110:517–536. http://dx.doi.org/10.1007/s00702-002-0808-2

Braak, H., E. Ghebremedhin, U. Rüb, H. Bratzke, and K. Del Tredici. 2004. Stages in the development of Parkinson's disease-related pathology. *Cell Tissue Res.* 318:121–134. http://dx.doi.org/10.1007/s00441-004-0956-9

Bruce, M., A. Chree, I. McConnell, J. Foster, G. Pearson, and H. Fraser. 1994. Transmission of bovine spongiform encephalopathy and scrapie to mice: strain variation and the species barrier. *Philos. Trans. R. Soc. Lond. B Biol. Sci.* 343:405–411. http://dx.doi.org/10.1098/rstb.1994.0036

Brunjes, P.C., and K.R. Illig. 2009. Anterior Olfactory Nucleus. *In* Encyclopedia of Neuroscience. Springer Berlin Heidelberg, Berlin Heidelberg. 128–131.

Burwell, R.D., M.P. Witter, and D.G. Amaral. 1995. Perirhinal and postrhinal cortices of the rat: a review of the neuroanatomical literature and comparison with findings from the monkey brain. *Hippocampus.* 5:390–408. http://dx.doi.org/10.1002/hipo.450050503

Chu, Y., and J.H. Kordower. 2015. The prion hypothesis of Parkinson's disease. *Curr. Neurol. Neurosci. Rep.* 15:28. http://dx.doi.org/10.1007/s11910-015-0549-x

Cinelli, A.R., H. Ferreyra-Moyano, and E. Barragan. 1987. Reciprocal functional connections of the olfactory bulbs and other olfactory related areas with the prefrontal cortex. *Brain Res. Bull.* 19:651–661. http://dx.doi.org/10.1016/0361-9230(87)90051-7

Cleland, T.A., A. Morse, E.L. Yue, and C. Linster. 2002. Behavioral models of odor similarity. *Behav. Neurosci.* 116:222–231. http://dx.doi.org/10.1037/0735-7044.116.2.222

Dehay, B., M. Vila, E. Bezard, P. Brundin, and J.H. Kordower. 2016. Alpha-synuclein propagation: New insights from animal models. *Mov. Disord.* 31:161–168. http://dx.doi.org/10.1002/mds.26370

De La Rosa-Prieto, C., M. De Moya-Pinilla, D. Saiz-Sanchez, I. Ubeda-Banon, D.M. Arzate, A. Flores-Cuadrado, T. Liberia, C. Crespo, and A. Martinez-Marcos. 2015. Olfactory and cortical projections to bulbar and hippocampal adult-born neurons. *Front. Neuroanat.* 9:4. http://dx.doi.org/10.3389/fnana.2015.00004

Del Tredici, K., and H. Braak. 2000. Idiopathic Parkinson's disease: staging an α-synucleinopathy with a predictable pathoanatomy. In Madame Curie Bioscience Database. Landes Bioscience, Austin, TX. Available at: http://www.ncbi.nlm.nih.gov/books/NBK6077/

Doty, R.L. ed. 2003. Handbook of Olfaction and Gustation. Marcel Dekker, Inc. 1172 pp.

Dunning, C.J.R., J.F. Reyes, J.A. Steiner, and P. Brundin. 2012. Can Parkinson's disease pathology be propagated from one neuron to another? *Prog. Neurobiol.* 97:205–219. http://dx.doi.org/10.1016/j.pneurobio.2011.11.003

Fujiwara, H., M. Hasegawa, N. Dohmae, A. Kawashima, E. Masliah, M.S. Goldberg, J. Shen, K. Takio, and T. Iwatsubo. 2002. alpha-Synuclein is phosphorylated in synucleinopathy lesions. *Nat. Cell Biol.* 4:160–164.

George, S., N.L. Rey, N. Reichenbach, J.A. Steiner, and P. Brundin. 2013. α-Synuclein: the long distance runner. *Brain Pathol.* 23:350–357. http://dx.doi.org/10.1111/bpa.12046

Giasson, B.I., M.S. Forman, M. Higuchi, L.I. Golbe, C.L. Graves, P.T. Kotzbauer, J.Q. Trojanowski, and V.M.Y. Lee. 2003. Initiation and synergistic fibrillization of tau and alpha-synuclein. *Science.* 300:636–640. http://dx.doi.org/10.1126/science.1082324

Goedert, M. 2001. Alpha-synuclein and neurodegenerative diseases. *Nat. Rev. Neurosci.* 2:492–501. http://dx.doi.org/10.1038/35081564

Guo, J.L., and V.M.Y. Lee. 2014. Cell-to-cell transmission of pathogenic proteins in neurodegenerative diseases. *Nat. Med.* 20:130–138. http://dx.doi.org/10.1038/nm.3457

Guo, J.L., D.J. Covell, J.P. Daniels, M. Iba, A. Stieber, B. Zhang, D.M. Riddle, L.K. Kwong, Y. Xu, J.Q. Trojanowski, and V.M.Y. Lee. 2013. Distinct α-synuclein strains differentially promote tau inclusions in neurons. *Cell.* 154:103–117. http://dx.doi.org/10.1016/j.cell.2013.05.057

Haehner, A., S. Boesveldt, H.W. Berendse, A. Mackay-Sim, J. Fleischmann, P.A. Silburn, A.N. Johnston, G.D. Mellick, B. Herting, H. Reichmann, and T. Hummel. 2009. Prevalence of smell loss in Parkinson's disease—a multicenter study. *Parkinsonism Relat. Disord.* 15:490–494. http://dx.doi.org/10.1016/j.parkreldis.2008.12.005

Höglinger, G.U., D. Alvarez-Fischer, O. Arias-Carrión, M. Djufri, A. Windolph, U. Keber, A. Borta, V. Ries, R.K.W. Schwarting, D. Scheller, and W.H. Oertel. 2015. A new dopaminergic nigro-olfactory projection. *Acta Neuropathol.* 130:333–348. http://dx.doi.org/10.1007/s00401-015-1451-y

Illig, K.R., and J.D. Eudy. 2009. Contralateral projections of the rat anterior olfactory nucleus. *J. Comp. Neurol.* 512:115–123. http://dx.doi.org/10.1002/cne.21900

Ishizawa, T., P. Mattila, P. Davies, D. Wang, and D.W. Dickson. 2003. Colocalization of tau and alpha-synuclein epitopes in Lewy bodies. *J. Neuropathol. Exp. Neurol.* 62:389–397. http://dx.doi.org/10.1093/jnen/62.4.389

Kelly, J.W. 1996. Alternative conformations of amyloidogenic proteins govern their behavior. *Curr. Opin. Struct. Biol.* 6:11–17. http://dx.doi.org/10.1016/S0959-440X(96)80089-3

Kranick, S.M., and J.E. Duda. 2008. Olfactory dysfunction in Parkinson's disease. *Neurosignals.* 16:35–40. http://dx.doi.org/10.1159/000109757

Krueger, C., and L. Tian. 2004. A comparison of the general linear mixed model and repeated measures ANOVA using a dataset with multiple missing data points. *Biol. Res. Nurs.* 6:151–157. http://dx.doi.org/10.1177/1099800404267682

Kuusisto, E., L. Parkkinen, and I. Alafuzoff. 2003. Morphogenesis of Lewy bodies: dissimilar incorporation of alpha-synuclein, ubiquitin, and p62. *J. Neuropathol. Exp. Neurol.* 62:1241–1253. http://dx.doi.org/10.1093/jnen/62.12.1241

Lamberts, J.T., E.N. Hildebrandt, and P. Brundin. 2014. Spreading of α-synuclein in the face of axonal transport deficits in Parkinson's disease: a speculative synthesis. *Neurobiol. Dis.* 77:276–283. http://dx.doi.org/10.1016/j.nbd.2014.07.002

Lavedan, C. 1998. The synuclein family. *Genome Res.* 8:871–880.

Li, J.-Y., E. Englund, H. Widner, S. Rehncrona, A. Björklund, O. Lindvall, and P. Brundin. 2010. Characterization of Lewy body pathology in 12- and 16-year-old intrastriatal mesencephalic grafts surviving in a patient with Parkinson's disease. *Mov. Disord.* 25:1091–1096. http://dx.doi.org/10.1002/mds.23012

Luk, K.C., C. Song, P. O'Brien, A. Stieber, J.R. Branch, K.R. Brundent, J.Q. Trojanowski, and V.M.-Y. Lee. 2009. Exogenous α-synuclein fibrils seed the formation of Lewy body-like intracellular inclusions in cultured cells. *Proc. Natl. Acad. Sci. USA.* 106:20051–20056. http://dx.doi.org/10.1073/pnas.0908005106

Luk, K.C., V. Kehm, J. Carroll, B. Zhang, P. O'Brien, J.Q. Trojanowski, and V.M.Y. Lee. 2012a. Pathological α-synuclein transmission initiates Parkinson-like neurodegeneration in nontransgenic mice. *Science.* 338:949–953. http://dx.doi.org/10.1126/science.1227157

Luk, K.C., V.M. Kehm, B. Zhang, P. O'Brien, J.Q. Trojanowski, and V.M.Y. Lee. 2012b. Intracerebral inoculation of pathological α-synuclein initiates a rapidly progressive neurodegenerative α-synucleinopathy in mice. *J. Exp. Med.* 209:975–986. http://dx.doi.org/10.1084/jem.20112457

Mahlknecht, P., K. Seppi, and W. Poewe. 2015. The Concept of Prodromal Parkinson's Disease. *J. Parkinsons Dis.* 5:681–697. http://dx.doi.org/10.3233/JPD-150685

Mandairon, N., S. Sultan, N. Rey, F. Kermen, M. Moreno, G. Busto, V. Farget, B. Messaoudi, M. Thevenet, and A. Didier. 2009. A computer-assisted odorized hole-board for testing olfactory perception in mice. *J. Neurosci. Methods.* 180:296–303. http://dx.doi.org/10.1016/j.jneumeth.2009.04.008

Masuda-Suzukake, M., T. Nonaka, M. Hosokawa, T. Oikawa, T. Arai, H. Akiyama, D.M.A. Mann, and M. Hasegawa. 2013. Prion-like spreading of pathological α-synuclein in brain. *Brain.* 136:1128–1138. http://dx.doi.org/10.1093/brain/awt037

Mougenot, A.-L., S. Nicot, A. Bencsik, E. Morignat, J. Verchère, L. Lakhdar, S. Legastelois, and T. Baron. 2012. Prion-like acceleration of a synucleinopathy in a transgenic mouse model. *Neurobiol. Aging.* 33:2225–2228. http://dx.doi.org/10.1016/j.neurobiolaging.2011.06.022

Moussaud, S., D.R. Jones, E.L. Moussaud-Lamodière, M. Delenclos, O.A. Ross, and P.J. McLean. 2014. Alpha-synuclein and tau: teammates in neurodegeneration? *Mol. Neurodegener.* 9:43. http://dx.doi.org/10.1186/1750-1326-9-43

Olanow, C.W., and S.B. Prusiner. 2009. Is Parkinson's disease a prion disorder? *Proc. Natl. Acad. Sci. USA.* 106:12571–12572. http://dx.doi.org/10.1073/pnas.0906759106

Osterberg, V.R., K.J. Spinelli, L.J. Weston, K.C. Luk, R.L. Woltjer, and V.K. Unni. 2015. Progressive aggregation of alpha-synuclein and selective degeneration of lewy inclusion-bearing neurons in a mouse model of parkinsonism. *Cell Reports.* 10:1252–1260. http://dx.doi.org/10.1016/j.celrep.2015.01.060

Oueslati, A. 2016. Implication of Alpha-Synuclein Phosphorylation at S129 in Synucleinopathies: What Have We Learned in the Last Decade? *J. Parkinsons Dis.* 6:39–51. http://dx.doi.org/10.3233/JPD-160779

Paumier, K.L., K.C. Luk, F.P. Manfredsson, N.M. Kanaan, J.W. Lipton, T.J. Collier, K. Steece-Collier, C.J. Kemp, S. Celano, E. Schulz, et al. 2015.

Intrastriatal injection of pre-formed mouse α-synuclein fibrils into rats triggers α-synuclein pathology and bilateral nigrostriatal degeneration. *Neurobiol. Dis.* 82:185–199. http://dx.doi.org/10.1016/j.nbd.2015.06.003

Paxinos, G., and K.B.J. Franklin. 2012. Paxinos and Franklin's The Mouse Brain in Stereotaxic Coordinates. Fourth edition. Elsevier Academic Press, London. 360 pp.

Peelaerts, W., L. Bousset, A. Van der Perren, A. Moskalyuk, R. Pulizzi, M. Giugliano, C. Van den Haute, R. Melki, and V. Baekelandt. 2015. α-Synuclein strains cause distinct synucleinopathies after local and systemic administration. *Nature.* 522:340–344. http://dx.doi.org/10.1038/nature14547

Postuma, R.B., D. Aarsland, P. Barone, D.J. Burn, C.H. Hawkes, W. Oertel, and T. Ziemssen. 2012. Identifying prodromal Parkinson's disease: pre-motor disorders in Parkinson's disease. *Mov. Disord.* 27:617–626. http://dx.doi.org/10.1002/mds.24996

Recasens, A., B. Dehay, J. Bové, I. Carballo-Carbajal, S. Dovero, A. Pérez-Villalba, P.-O. Fernagut, J. Blesa, A. Parent, C. Perier, et al. 2014. Lewy body extracts from Parkinson disease brains trigger α-synuclein pathology and neurodegeneration in mice and monkeys. *Ann. Neurol.* 75:351–362. http://dx.doi.org/10.1002/ana.24066

Rey, N.L., D. Jardanhazi-Kurutz, D. Terwel, M.P. Kummer, F. Jourdan, A. Didier, and M.T. Heneka. 2012a. Locus coeruleus degeneration exacerbates olfactory deficits in APP/PS1 transgenic mice. *Neurobiol. Aging.* 33:426.e1–426.e11. http://dx.doi.org/10.1016/j.neurobiolaging.2010.10.009

Rey, N.L., J. Sacquet, A. Veyrac, F. Jourdan, and A. Didier. 2012b. Behavioral and cellular markers of olfactory aging and their response to enrichment. *Neurobiol. Aging.* 33:626.e9–626.e23. http://dx.doi.org/10.1016/j.neurobiolaging.2011.03.026

Rey, N.L., G.H. Petit, L. Bousset, R. Melki, and P. Brundin. 2013. Transfer of human α-synuclein from the olfactory bulb to interconnected brain regions in mice. *Acta Neuropathol.* 126:555–573. http://dx.doi.org/10.1007/s00401-013-1160-3

Rey, N.L., S. George, and P. Brundin. 2016. Review: Spreading the word: precise animal models and validated methods are vital when evaluating prion-like behaviour of alpha-synuclein. *Neuropathol. Appl. Neurobiol.* 42:51–76. http://dx.doi.org/10.1111/nan.12299

Sacino, A.N., M. Brooks, M.A. Thomas, A.B. McKinney, S. Lee, R.W. Regenhardt, N.H. McGarvey, J.I. Ayers, L. Notterpek, D.R. Borchelt, et al. 2014. Intramuscular injection of α-synuclein induces CNS α-synuclein pathology and a rapid-onset motor phenotype in transgenic mice. *Proc. Natl. Acad. Sci. USA.* 111:10732–10737. http://dx.doi.org/10.1073/pnas.1321785111

Sah, P., E.S. Faber, M. Lopez De Armentia, and J. Power. 2003. The amygdaloid complex: anatomy and physiology. *Physiol. Rev.* 83:803–834. http://dx.doi.org/10.1152/physrev.00002.2003

Shi, C.J., and M.D. Cassell. 1998. Cascade projections from somatosensory cortex to the rat basolateral amygdala via the parietal insular cortex. *J. Comp. Neurol.* 399:469–491. http://dx.doi.org/10.1002/(SICI)1096-9861(19981005)399:4<469::AID-CNE3>3.0.CO;2-#

Slotnick, B.M., S. Graham, D.G. Laing, and G.A. Bell. 1987. Detection of propionic acid vapor by rats with lesions of olfactory bulb areas associated with high 2-DG uptake. *Brain Res.* 417:343–346. http://dx.doi.org/10.1016/0006-8993(87)90460-4

Ulusoy, A., R.E. Musgrove, R. Rusconi, M. Klinkenberg, M. Helwig, A. Schneider, and D.A. Di Monte. 2015. Neuron-to-neuron α-synuclein propagation in vivo is independent of neuronal injury. *Acta Neuropathol. Commun.* 3:13. http://dx.doi.org/10.1186/s40478-015-0198-y

Volpicelli-Daley, L.A., K.C. Luk, and V.M.Y. Lee. 2014. Addition of exogenous α-synuclein preformed fibrils to primary neuronal cultures to seed recruitment of endogenous α-synuclein to Lewy body and Lewy neurite-like aggregates. *Nat. Protoc.* 9:2135–2146. http://dx.doi.org/10.1038/nprot.2014.143

Wesson, D.W., and D.A. Wilson. 2011. Sniffing out the contributions of the olfactory tubercle to the sense of smell: hedonics, sensory integration, and more? *Neurosci. Biobehav. Rev.* 35:655–668. http://dx.doi.org/10.1016/j.neubiorev.2010.08.004

Wilson, D.A., and M. Leon. 1987. Evidence of lateral synaptic interactions in olfactory bulb output cell responses to odors. *Brain Res.* 417:175–180. http://dx.doi.org/10.1016/0006-8993(87)90196-X